



Water Resources Research

RESEARCH ARTICLE

10.1002/2017WR021205

Key Points:

- Attribution of long-lead large-scale climate signals to seasonal peak-flow is identified globally
- Season-ahead seasonal peak-flow prediction models are constructed globally
- Fair-to-good prediction skill is evident for many locations, most notably data-poor regions (e.g., West and Central Africa)

Supporting Information:

- Supporting Information S1

Correspondence to:

P. Block,
paul.block@wisc.edu

Citation:

Lee, D., Ward, P., & Block, P. (2018). Attribution of large-scale climate patterns to seasonal peak-flow and prospects for prediction globally. *Water Resources Research*, 54, 916–938.
<https://doi.org/10.1002/2017WR021205>

Received 27 MAY 2017

Accepted 6 JAN 2018

Accepted article online 11 JAN 2018

Published online 9 FEB 2018

Attribution of Large-Scale Climate Patterns to Seasonal Peak-Flow and Prospects for Prediction Globally

Donghoon Lee¹ , Philip Ward² , and Paul Block¹ 

¹Department of Civil and Environmental Engineering, University of Wisconsin-Madison, Madison, Wisconsin, USA, ²Department of Water and Climate Risk, Institute for Environmental Studies, Vrije Universiteit Amsterdam, Amsterdam, The Netherlands

Abstract Flood-related fatalities and impacts on society surpass those from all other natural disasters globally. While the inclusion of large-scale climate drivers in streamflow (or high-flow) prediction has been widely studied, an explicit link to global-scale long-lead prediction is lacking, which can lead to an improved understanding of potential flood propensity. Here we attribute seasonal peak-flow to large-scale climate patterns, including the El Niño Southern Oscillation (ENSO), Pacific Decadal Oscillation (PDO), North Atlantic Oscillation (NAO), and Atlantic Multidecadal Oscillation (AMO), using streamflow station observations and simulations from PCR-GLOBWB, a global-scale hydrologic model. Statistically significantly correlated climate patterns and streamflow autocorrelation are subsequently applied as predictors to build a global-scale season-ahead prediction model, with prediction performance evaluated by the mean squared error skill score (MSESS) and the categorical Gerrity skill score (GSS). Globally, fair-to-good prediction skill ($20\% \leq \text{MSESS} \leq 0.2 \leq \text{GSS}$) is evident for a number of locations (28% of stations and 29% of land area), most notably in data-poor regions (e.g., West and Central Africa). The persistence of such relevant climate patterns can improve understanding of the propensity for floods at the seasonal scale. The prediction approach developed here lays the groundwork for further improving local-scale seasonal peak-flow prediction by identifying relevant global-scale climate patterns. This is especially attractive for regions with limited observations and/or little capacity to develop flood early warning systems.

1. Introduction

Flood-related fatalities, economic damages, and impacts on society surpass those from all other natural disasters globally (Doocy et al., 2013; Munich Re, 2012). Flood forecasts and early warning systems integrated with emergency planning and management have lessened mortality and damages (Golnaraghi et al., 2009; Radziejewski & Kundzewicz, 2004); however, the need remains for additional early warning systems to foster improved flood preparedness. There is a particular lack of seasonal-scale flood forecasts to complement more typical short-range forecasts (hours to days). While short-range forecasts are critical to warn of imminent danger, seasonal-scale forecasts can provide longer time leads to facilitate proactive decision-making. For example, the International Federation of Red Cross (IFRC) has highlighted the applicability of seasonal forecasts for preflood decisions, such as prepositioning relief supplies, maintaining facilities, and increasing volunteer numbers (IFRC, 2011). Seasonal forecasts can also inform reservoir operations for flood management (Chiew et al., 2003; Ritchie et al., 2004; Sankarasubramanian & Lall, 2003).

Some operational centers have developed medium range (10–45 days) continental-scale or global-scale hydrological ensemble prediction systems (HEPS) using numerical weather prediction model outputs and large-scale hydrological models. For example, the Global Flood Awareness System (GloFAS), jointly developed by the European Commission and the European Centre for Medium-range Weather Forecasting (ECMWF), uses meteorological forcings from the ensemble prediction system of ECMWF with the Hydrologically modified ECMWF Tiled Scheme for Surface Exchanges over Land and the LISFLOOD channel routing model to forecast probabilistic exceedance of streamflow (Alfieri et al., 2013). The U.S. National Weather Service operates the Hydrologic Ensemble Forecast Service over the contiguous United States using medium range forecasts (from the National Centers for Environmental Prediction) and their hydrologic processor (Demargne et al., 2014). Other operational large-scale HEPSs are reviewed in Emerton et al. (2016).

The HEPSs can provide specific information, such as hydrographs and frequencies at fine temporal scales; however, the uncertainty of EPS forecasts increases with longer lead time due to chaotic evolution of the

atmospheric system (Doblas-Reyes et al., 2013; Palmer, 2000; Westra & Sharma, 2010). In addition, their skillful lead time is typically not sufficient for long-range disaster management (weeks-months), particularly for developing regions evaluating disaster preparedness options.

In relation to this, numerous studies have illustrated significant relationships between streamflow/hydrological conditions (average and extremes, e.g., floods and droughts) and large-scale climate patterns (e.g., El Niño Southern Oscillation (ENSO)), providing prospects for skillful seasonal forecasts and flood management (Burn & Arnell, 1993; Cayan et al., 1999; Chiew & McMahon, 2002; Dettinger et al., 2000, 2001; Pizarro & Lall, 2002; Tootle et al., 2005; Ward et al., 2014b). However, only a limited number of studies have investigated continental or global scale applications. For example, Chiew and McMahon (2002) demonstrate an ENSO teleconnection with global streamflow using harmonic analysis and lag-correlations in 581 catchments by applying the Southern Oscillation Index (SOI) and Multivariate ENSO Index (MEI). Bierkens and van Beek (2009) utilize predictions of the wintertime North Atlantic Oscillation (NAO) Index, NAO-associated meteorological and hydrological conditions, and a global hydrological model to evaluate the seasonal predictability of streamflow over the European continent. Tootle et al. (2005) show significant relationships between continental U.S. annual streamflow and ENSO, Pacific Decadal Oscillation (PDO), North Atlantic Oscillation (NAO), Atlantic Multidecadal Oscillation (AMO), and their coupled patterns using a nonparametric significance test. McCabe and Wolock (2008) and Dettinger et al. (2000) find leading modes of variability (principal components) associated with ENSO and North Atlantic sea surface temperatures (SST) when performing a principal components analysis (PCA) on global streamflow and Western hemisphere streamflow, respectively. Ward et al. (2010, 2014a) highlight the significant influence of ENSO on the sensitivity of flood duration and frequency globally using correlation and regression analysis, leading to anomalies in flood risk for many parts of the world. Emerton et al. (2017) also emphasize the role of ENSO on potential flood risks globally by providing the historical probability of abnormally high or low monthly streamflow during El Niño and La Niña events and subsequent increased or decreased flood hazard based on the reconstructed global streamflow for the twentieth century.

While these studies demonstrate the relationship between individual or multiple large-scale climate patterns and annual or seasonal streamflow or the likelihood of climate-driven extreme streamflow globally (Emerton et al., 2017), there is no explicit link to the predictability of seasonal streamflow. Therefore, a need exists to expand such analyses to target long-range streamflow prediction using large-scale climate drivers at the global scale, motivated by the potential to provide useful information for flood management.

In this study, we attribute year-to-year variation in seasonal peak-flow, defined as average streamflow across the peak (3 month) season, to large-scale climate patterns and subsequently build a global-scale season-ahead prediction model conditioned on these patterns. Both attribution and prediction are performed with extensive streamflow observations and simulations from a global hydrological model to cover data-scarce regions.

2. Data and Methods

First, we describe the process of setting up streamflow observations and simulations. For attribution, we evaluate correlations between seasonal streamflow (peak-flow season) and large-scale interannual and interdecadal climate drivers (ENSO, PDO, NAO, and AMO at 3–8 months lead time) as well as streamflow autocorrelation. From the suite of potential (significantly correlated) predictors, an optimal lead-months of climate predictors is determined using a cross validation criteria and a linear regression model is applied to predict seasonal peak-flow at each location, including performance and verification metrics.

2.1. Data

To establish climate-induced variability in streamflow, it is valuable to consider natural streamflow records, since regulation of dams and reservoirs may produce spurious relationships that may misalign with management objectives. Seasonal peak-flow is often regulated by dam managers distributing streamflow across multiple seasons or releasing preseason storage causing an overestimation of downstream flows. In the data section, we describe the criteria for retaining natural streamflow stations and “allowable” regulated stations (e.g., dam inflow) that might be useful for reservoir management decision-making. Also, reconstructed streamflow simulations are used to identify climate-streamflow relationships where observations do not exist. In this study, streamflow observations are mainly used for gauged areas, and streamflow simulations are used for ungauged (data-limited) regions.

2.1.1. Streamflow Observations

For this study, streamflow observations were obtained from the Global Runoff Data Centre (GRDC) (Global Runoff Data Centre, 2007) and the U.S. Geological Survey (USGS). Given our interest in examining hydro-climatic relationships, it is important to select unimpaired streamflow stations for analysis. Stations located in the downstream reaches of large-scale river basins may be regulated by water supply, flood control, irrigation, hydropower infrastructure (World Commission on Dams, 2000), etc., potentially altering flow regimes (from natural to regulated) drastically. Identifying such infrastructure is thus important. Globally more than 33,000 large reservoirs and dams are listed (International Commission on Large Dams, 2009), with geo-referencing available for 6,862 of them (Lehner et al., 2011). Lehner et al. (2011) also found that nearly 47% of large rivers with average streamflow in excess of 1,000 m³/s are significantly regulated by dams, attenuating flow hydrographs, and flood volumes. Another important aspect to address is that streamflow in some upstream reaches is more sensitive to local weather and hydrologic conditions, which can suppress large-scale climatic impacts, depending on the climatic and hydrogeographic characteristics of the specific location. Finally, many poorly gauged regions have limited observations and may be excluded if strict rules are applied (e.g., minimum catchment size or length of observational record), resulting in an uneven global distribution. Thus, to properly collect records from unimpaired stations, and coincidentally minimize location bias globally, we apply a flexible and robust selection criteria.

We start by selecting GRDC stations having at least 30 years of streamflow observations (either daily or monthly) across any time period, allowing more stations to be retained globally and particularly in data-limited regions. We assume that streamflow-climate relationships do not significantly vary in time, that is, streamflow observations in different time periods (windows) illustrate similar relationship and predictability with season-ahead climate drivers. With a minimum catchment area larger than 10,000 km², which is arbitrarily defined to exclude stations relatively sensitive to regional climate and anthropogenic impacts, 2,203 GRDC stations globally are selected. All selected GRDC stations are then mapped to corresponding grids in the global 30 min river network (Döll & Lehner, 2002).

The impact of dams on streamflow varies depending on station location, distance from a dam, dam capacity, operating rules, etc., thus just because a station is located downstream of a dam, it should not automatically be classified as impaired or regulated. Therefore, we first investigate the locations of all dams and reservoirs in each basin to divide stations into two categories: unregulated (no dams or reservoirs upstream) and regulated (dams or reservoirs exist upstream). This is done by digitally mapping all dams near the selected stations from the Global Reservoir and Dam database (GranD) (Lehner et al., 2011) and the HydroLAKES data set (Messager et al., 2016) using the high-resolution global river network and basin delineation from HydroSHEDS (Lehner et al., 2008). Next we assess the magnitude of regulation from upstream dams or reservoirs on changes in streamflow climatology, seasonality, and attenuation of peak-flow (if any) across the observational record by visually inspecting all available year-to-year daily and monthly streamflow patterns at each station. The level of streamflow regulation is divided into four classes (none, allowable, regulated, and unusable), according to the following:

1. if streamflow climatology or seasonality is strongly regulated by upstream dams, the station is classified as *unusable*;
2. if streamflow climatology or seasonality is moderately regulated by upstream dams, the station is classified as *regulated*;
3. if streamflow climatology or seasonality is minimally regulated by small or distant dams, the station is classified as *allowable*; and
4. if no dam is located upstream, the station is classified as *none*.

This screening process, while structured, is not purely objective but arguably appropriate for this hydroclimatological context focusing on seasonal peak-flow, given the similarity in classification results to the degree of regulation of global rivers identified in Lehner et al. (2011). To retain natural streamflow and “allowable” regulated streamflow, which might be useful for reservoir management, we only select stations with none and allowable regulation categories. As a result, the screening process produces 616 (331) GRDC stations with none (allowable) regulation containing at least 30 years of observations (947 GRDC stations in total).

Using this screening process, many stations in the western and southeastern U.S., well-known as climate-sensitive regions, are excluded due to highly regulated mean streamflow or peak-flow. To provide coverage for these regions, we additionally include data from the USGS Hydro-Climatic Data Network (HCDN) (Lins,

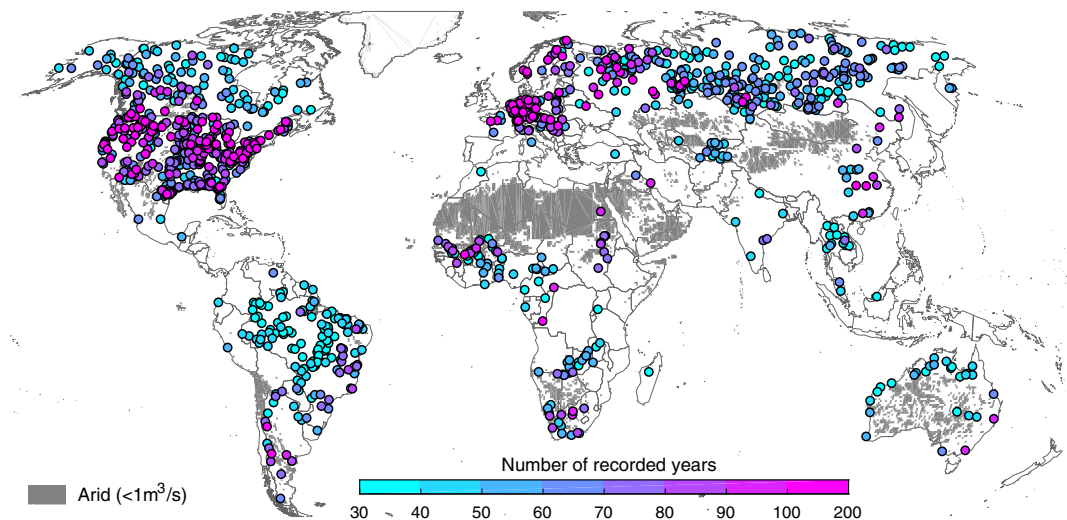


Figure 1. Location of 1,200 stations (947 GRDC + 253 HCDN) with the numbers of recorded years per station.

2012), which lists prevalidated USGS stations that meet strict selection criteria, even including human activities. We select 253 HCDN stations with at least 30 years of observations and minimum catchment areas larger than 500 km^2 . Thus in total, we select 1,200 stations globally (947 GRDC + 253 HCDN), with an average station record length of 65 years and good global spatial distribution (Figure 1).

Annual streamflow statistics (maximum or mean value in the water year) are often used to analyze streamflow variations associated with large-scale climate patterns in global studies. For estimating flood propensity at the seasonal scale, it is important to identify and define seasonal streamflow in the dominant flood season. Although a high-flow value (seasonal maximum or upper percentile streamflow) may represent a more traditional flood characterization, this value may also include variability due to local climate/hydrology may potentially be more significant than those from season-ahead large-scale climate drivers. For this study, we use seasonal peak-flow, calculated as average streamflow in the peak (3 month) season according to the volume-based threshold method and daily streamflow data, as defined in Lee et al. (2015). Daily gridded streamflow is obtained from the PCR-GLOBWB (PCRaster GLObal Water Balance) model, described in the following section; peak-flow seasons (Figure 2) are validated with corresponding GRDC streamflow observations and actual flood records.

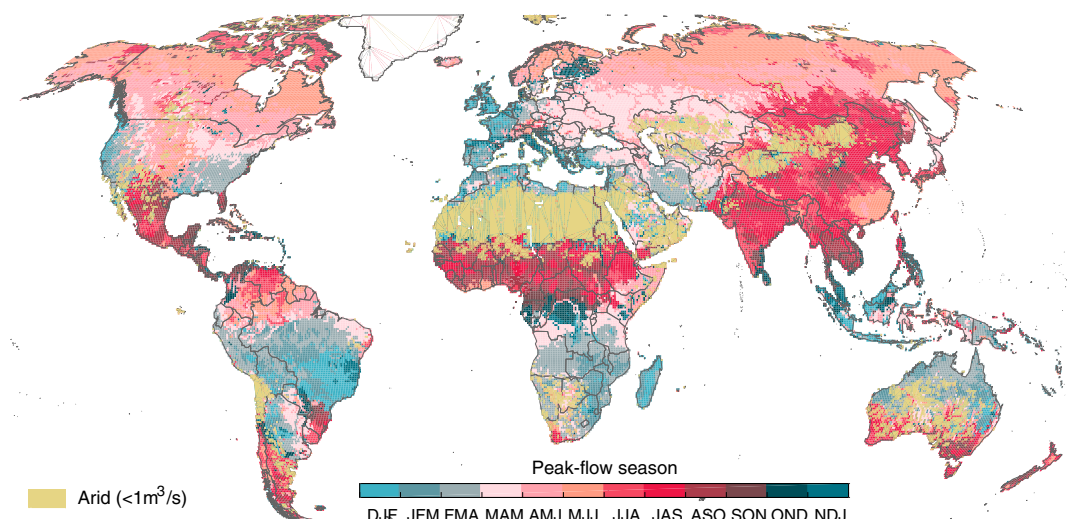


Figure 2. Peak-flow season defined using the volume-based threshold method with streamflow simulations from the PCR-GLOBWB model (Lee et al., 2015).

2.1.2. Global Streamflow Simulation

Even though considerable effort has been devoted to selecting a sufficient number of stations to provide global coverage (Figure 1), a dearth of stations exists in locations that are often considered vulnerable to natural disasters, and where global long-term predictions may be extremely useful (e.g., sub-Saharan Africa). This can be partially resolved by adopting spatially continuous streamflow data simulated by a global hydrological model and treating these time series as pseudo-observations. Here we utilize daily streamflow simulations over the period 1958–2000 (43 years) from Ward et al. (2013), reproduced using PCR-GLOBWB, a global hydrological model with a spatial resolution of $0.5^\circ \times 0.5^\circ$ (Van Beek & Bierkens, 2009; Van Beek et al., 2011; Winsemius et al., 2013), validated on streamflow quantity (Van Beek et al., 2011), and terrestrial water storage (Wada et al., 2011) for numerous major rivers in the world. Extreme discharge values produced by the model have also been compared with station data (Ward et al., 2013), performing generally well for large drainage areas. For the simulations considered in this study, the PCR-GLOBWB model used daily meteorological forcing data from the Water and Global Change (WATCH) project (Weedon et al., 2011), including precipitation, temperature, and global radiation data. The WATCH forcing data were initially derived from the ERA-40 reanalysis product (Uppala et al., 2005), and subjected to corrections based on precipitation gauges, elevation, time adjustments to reflect monthly observations from daily values, and varying atmospheric aerosol loadings. Also, the model is simulated without a reservoir scheme to produce natural streamflow. Using PCR-GLOBWB streamflow time series globally, we follow an identical approach as with the GRDC observations to construct seasonal peak-flow, averaging streamflow in the predefined peak season (Lee et al., 2015) for each grid globally.

Normality of log-transformed seasonal peak-flow is assessed using the Lilliefors test on both observed and simulated data. As a result, 77% of observed stations and 84% of global land areas, excluding Antarctica, Greenland, and dry regions, show significant log-normality at the 95% significance level (supporting information Figure S1). Based on this fairly high percentage of stations and areas illustrating significant log-normality, we apply log-transformations to all streamflow data prior to developing the prediction (linear regression) models globally.

2.1.3. Large-Scale Climate Index Data

For this study, four interannual, decadal, and interdecadal climatic indicators are evaluated: ENSO, PDO, NAO, and AMO.

The El Niño Southern Oscillation (ENSO) is a periodic fluctuation (every 2–7 years) in sea surface temperature (El Niño or La Niña) and air pressure system (Southern Oscillation) over the equatorial Pacific Ocean and surrounding regions. In the El Niño (warm) phase, areas of the western Pacific (southeast Asia, Australia, and South Africa) experience abnormal drought, while heavy precipitation occurs in the eastern Pacific (west coast and south east of the U.S.). The approximate opposite climate pattern occurs in the La Niña (cold) phase over the same regions (Ropelewski & Halpert, 1986, 1987). To represent ENSO, we use the Nino 3.4 index (3 month running mean of average sea surface temperature (SST) over 5°N – 5°S , 120°W – 170°W ; https://www.esrl.noaa.gov/psd/gcos_wgsp/Timeseries/Nino34/), which captures classical ENSO events in the equatorial Pacific Ocean. We acknowledge that different types of ENSO (e.g., Eastern Pacific or Central Pacific El Niño) may have distinctly different impacts on precipitation and subsequent streamflow globally (Liang et al., 2016), yet those variations or other common ENSO indices are not evaluated here.

The Pacific Decadal Oscillation (PDO) is a fluctuation of North Pacific sea surface temperature that often presents as an ENSO-like pattern of Pacific climate variability. However, PDO varies over a much longer timescale (decades) compared to ENSO (interannual), with strong effects on North America (Zhang et al., 1997). For example, the positive (warm) phase of PDO is associated with above-normal temperature along the North American west coast and northeastern South America, above-normal precipitation over southwestern United States, and below-normal temperature and precipitation across the southeastern United States. The negative (cool) phase of PDO acts in an approximately opposite pattern (Mantua & Hare, 2002). The monthly PDO index (the leading principal component of monthly SST anomalies for the North Pacific basin north of 20°N) (Zhang et al., 1997) is obtained from the Joint Institute for the Study of the Atmosphere and Ocean (<http://research.jisao.washington.edu/pdo/>).

The North Atlantic Oscillation (NAO) is a semiperiodic oscillation in atmospheric surface pressure between the Subtropical (Azores) High and the Subpolar Low. The NAO affects the strength and location of the North Atlantic jet stream (westerly winds) and storm tracks across the Atlantic and into Europe, particularly in

winter, which results in variations of precipitation and temperature patterns from eastern North America to western and central Europe. The positive phase of the NAO (higher pressure in the Azores) is associated with below-normal precipitation over southern and central Europe and above-normal precipitation over northern Europe. The negative phase of the NAO reflects the opposite pattern of precipitation anomalies over these regions. For the NAO index, we use Hurrell's station-based seasonal NAO index (difference in normalized seasonal sea level pressure at Reykjavik and Lisbon stations) (Hurrell & Deser, 2009), obtained from the National Center for Atmospheric Research (<https://climatedataguide.ucar.edu/climate-data/hurrell-north-atlantic-oscillation-nao-index-station-based>).

The Atlantic Multidecadal Oscillation (AMO) index is defined as detrended area-weighted average SST over the North Atlantic (95°W–30°E, 0°N–70°N) with variability at multidecadal timescales (e.g., 65–80 year cycle for 1856–1999; warm phase during 1860–1880 and 1940–1960, and cold phase during 1905–1925 and 1970–1990) (Enfield et al., 2001). The positive (warm) phase of the AMO is associated with below-normal precipitation in the central U.S. and eastern South America and with above-normal precipitation in central Africa (Sahel) and Europe. The approximately opposite pattern occurs in the negative (cool) phase of the AMO (Knight et al., 2006). For the AMO index, we use the detrended and unsmoothed monthly AMO index calculated from Kaplan SST and obtained from https://www.esrl.noaa.gov/psd/gcos_wgsp/Timeseries/AMO.

For monthly PDO and AMO indices, we apply 3 month running means to represent seasonal persistence for the middle month of the season.

2.2. Methods

Here streamflow and climate indices are detrended and normalized prior to correlation analysis and prediction model development to avoid spurious relationships.

2.2.1. Covariability of Streamflow and Climate Drivers

We evaluate covariability between individual large-scale climate patterns and peak-flow using lagged correlations on the order of 3–8 months; since all predictions are based on 3 month averages (post 3 month running mean is applied for monthly PDO and AMO indices), 1–2 month lead time predictions are excluded given their overlap with the target season. Although streamflow and large-scale climate patterns are known to exhibit nonlinear relationships in some places, we simply calculate Pearson's correlations for evaluating the general strength of linear association and eventually for the linear regression prediction model. The correlation may account for both interannual and long-term (decadal and multidecadal for PDO and AMO, respectively) variations of climate drivers if present in a record period, however, considering the length of streamflow records (stations with 30–40 years records and 43 years for simulation) and removed linear trends, a large portion of covariability will be expected at the interannual scale. Each individual climate pattern (index) showing the maximum lag-correlation is retained as a potential predictor. Only statistically significant ($\alpha = 0.05$; *t* test) correlations are considered.

2.2.2. Streamflow Autocorrelation

Streamflow autocorrelation here refers to the relationship between streamflow from one season to the next. This persistence often allows season-ahead streamflow to act as a strong predictor of current season streamflow (Piechota et al., 1998). Streamflow autocorrelation for short lags (e.g., season) has also been demonstrated to be higher than the correlation between streamflow and ENSO in many catchments globally (Chiew & McMahon, 2002). Here we calculate the autocorrelation between streamflow in the season (3 months ahead) prior to the peak season at each station and grid globally. As with the climate drivers analysis, only season-ahead streamflow that is statistically significantly correlated is retained as a potential predictor.

2.2.3. Seasonal Peak-Flow Prediction

Given the suite of potential predictors having significant linear relationships with seasonal peak-flow, including large-scale climate drivers and streamflow autocorrelation, we apply a linear regression model to predict seasonal peak-flow. Predictors may conceivably be multicollinear (i.e., mutual correlations between predictors) containing redundant information and potentially leading to poor estimates of the regression parameters (Wilks, 2011). Therefore, if a single predictor (climate driver or streamflow autocorrelation) exists, we apply a linear regression model; if there are multiple predictors (either climate drivers or streamflow autocorrelation), we apply a Principal Component Regression (PCR) model to avoid possible multicollinearities. The PCR model has an identical form to Multiple Linear Regression (MLR); however, PCR uses Principal Components (PC), which are transformations of predictor variables and uncorrelated with each other, in

place of the raw predictor variables. By adding or removing uncorrelated PCs, the PCR model can retransform biased regression coefficients to the original predictor variables in the form of the MLR. If all PCs are retained, PCR is consistent with MLR (Wilks, 2011).

Generally, in the PCR process, the number of PCs retained as predictors is conditioned on the accumulated variance explained. Jolliffe (2002) suggests 70–90% may often be a reasonable range (Wilks, 2011). Here we truncate only the last PC with the smallest variance, which is also associated with multicollinearities if present (Jolliffe, 2002; Wilks, 2011). Although this rule may be strict for the case of a small number of predictor variables (e.g., two climate drivers have only two PCs), we apply to all PCR models globally for consistency. After truncating the last PC, the average accumulated variance explained of the remaining PCs is 78% and 75% for all observed and simulated streamflow, respectively. Thus it appears that this truncation rule is appropriately applied to the PCR model in terms of variance explained and eliminating possible multicollinearities.

Although we identified specific lead-months of climate drivers showing the maximum correlations with seasonal peak-flow, this may constrain the prediction model to discount a potential predictability from the predictors with different lead-months and account a possible large variance in the last PC, which will be eventually removed in the process of PCR model. Therefore, we applied the Leave-one-out Cross Validation (LOOCV) to find optimal lead times of the climate predictors. All combinations of lead-months (3–8 months ahead) for the climate predictors are cross-validated with a block size of 3 years and the PCR model. In each step of the LOOCV, we detrended and normalized all predictor and predictand variables to avoid potential source of dependence and artificial skill. From the cross validation, the combination of lead-months with the minimum Mean Squared Error (MSE) is selected as optimal lead-months.

Given the limited length of streamflow records available, it is important to carefully select the appropriate length of calibration and validation data to balance model confidence and reliability. Here we analyze prediction models with various lengths of calibration data, ranging from 50% to 100% starting from the first year of data. Selecting a 70% calibration data length, for example, implies that the first 70% of the streamflow record (i.e., first 30 years) is applied for model calibration and the remaining 30% (i.e., last 13 years) is used for model validation. Subsequently, model performance and calibration/validation data length are compared across each level.

Peak-flow may be highly related to prior-season streamflow, which is also linked to longer season-ahead prevailing climate conditions. Therefore, streamflow autocorrelation is likely already influenced by climate drivers and subsequently effects optimal lead-month selection and regression throughout the LOOCV and the PCR model. From an operational standpoint, including autocorrelated streamflow into the prediction model is practical and will potentially provide higher prediction skill. However, one can also develop prediction models conditioned only on climate predictors to identify locations with strong climate-driven predictability of seasonal peak-flow and compare with models explicitly including prior-season streamflow. We evaluate both, with models utilizing only climate predictors identified from the correlation analysis (Type-A) and models utilizing climate predictors and streamflow autocorrelation (Type-B).

2.2.4. Assessment of Prediction Skill

Two skill scores are used to evaluate prediction performance in different perspectives: the mean squared error skill score (MSESS) for performance in deterministic prediction and the Gerrity skill score (GSS) for performance in categorical prediction.

The MSESS is a relative skill score comparing MSE from predictions and MSE from climatology, and defined as follows (Wilks, 2011):

$$\text{MSESS} = \left(1 - \frac{\text{MSE}_{\text{pred}}}{\text{MSE}_{\text{clim}}} \right) \times 100\% \quad (1)$$

where MSE_{pred} is the MSE of prediction and MSE_{clim} is the MSE obtained from always predicting the climatological mean. Here an average of calibration data is used for the climatological mean for the validation period. The maximum value for the MSESS is 1, indicating a perfect prediction; a value of 0 indicates a model prediction skill equal to that of the climatological mean prediction. A negative value implies that the model prediction skill is worse than climatology, in terms of MSE (Jolliffe & Stephenson, 2012). The MSESS is considered as the main deterministic verification score for long-range forecasts in World Meteorological Organization (2007).

The GSS is a multicategorical skill score and contains an “equitability” (Gandin & Murphy, 1992) by rewarding correct predictions and penalizing incorrect ones. For a three-category prediction, the GSS is calculated as:

$$\text{GSS} = \sum_{i=1}^3 \sum_{j=1}^3 p_{ij} s_{ij} \quad (2)$$

where p_{ij} is the joint probability of events falling in category (i,j) and s_{ij} is the scoring weights. Gerrity (1992) proposed the approach to define scoring weights based on the sample climatology and odds ratios resulting in more credits for rarer events (low frequency) and fewer credits for common events (high frequency). The GSS ranges from -1 to 1 , where a value of 0 indicates no predictive skill compared with climatology and a value of 1 represents a perfect forecast. Negative values indicate model predictions worse than climatology. In this study, three categories are defined as the upper, middle, and lower thirds of the streamflow during the model calibration period.

Here we subjectively classify prediction performance according to a range of skill scores:

1. Poor prediction: $\text{MSESS} < 20\%$ and $\text{GSS} < 0.2$
2. Fair prediction: $20\% \leq \text{MSESS} < 60\%$ and $0.2 \leq \text{GSS} < 0.6$
3. Good prediction: $60\% \leq \text{MSESS}$ and $0.6 \leq \text{GSS}$

Note that above the thresholds are selected arbitrarily; however, considering these are seasonal streamflow predictions at the global scale with only 1–5 predictors, deterministic and categorical prediction with 20% (40%) higher skill than climatology could be regarded as fair (good) prediction. Also, the skill score ranges as defined are relatively higher than previous studies using these skill scores for seasonal streamflow prediction at the given location (Hidalgo-Muñoz et al., 2015). For this study, a prediction with fair performance is regarded as a useful prediction that may provide information to water management decisions and lead toward improved prediction models; a prediction with good performance is regarded as a practical prediction that may be applied in an operational sense for seasonal peak-flow prediction. The percentage of global areas with fair or good prediction performance is calculated by weighting the grids with the cosine of the latitude and excluding Antarctica, Greenland, and dry regions with streamflow less than $10 \text{ m}^3/\text{s}$.

3. Results and Discussion

In this section, we discuss attribution of the large-scale climate indices to seasonal peak-flow and their statistical significance, the importance of autocorrelation, and prediction results with verification metrics.

3.1. Attribution of Streamflow Variability to Large-Scale Climatic Indices

The maximum lag-correlation between seasonal peak-flow and season-ahead large-scale climate drivers (e.g., 0.4), the corresponding number of lead-months (e.g., 5 months), and the corresponding lead season (e.g., June–August) are determined globally (Figures 3–6) for both streamflow observations (GRDC and HCDN) and simulations (PCR-GLOBWB). Statistically significant relationships are primarily based on streamflow observation, where present, otherwise streamflow simulations are used to identify relationships, typically in data-limited areas.

3.1.1. ENSO Influence on Seasonal Peak-Flow Globally

Not surprisingly, high correlations are evident for regions with well-established ENSO signal-precipitation relationships (Dai & Wigley, 2000; Mason & Goddard, 2001) for both observed and simulated streamflow (Figure 3a). For example, negative correlations are observed in areas where La Niña induces above-normal precipitation in southwestern Canada and the northwestern U.S., northeastern South America (Amazon River basin), North and East Australia, Southeast Asia (no observed stations), and West, South, and East Africa. Positive correlations are observed in regions where El Niño induces above-normal precipitation in the southwestern and southeastern U.S., southeastern South America, Europe, and eastern Central Asia (Kyrgyzstan and Tajikistan) and South Russia. Correlations that exceed ENSO-precipitation correlations in many regions are also consistent with previous results for the western U.S. (Cayan et al., 1999) and at the global scale (Dettinger & Diaz, 2000), suggesting that direct streamflow response and association to climate teleconnections may be greater than precipitation or temperature. Since seasonal peak-flow has characteristics of both seasonal timescale and magnitude, the identified relationships can include both spatial patterns of

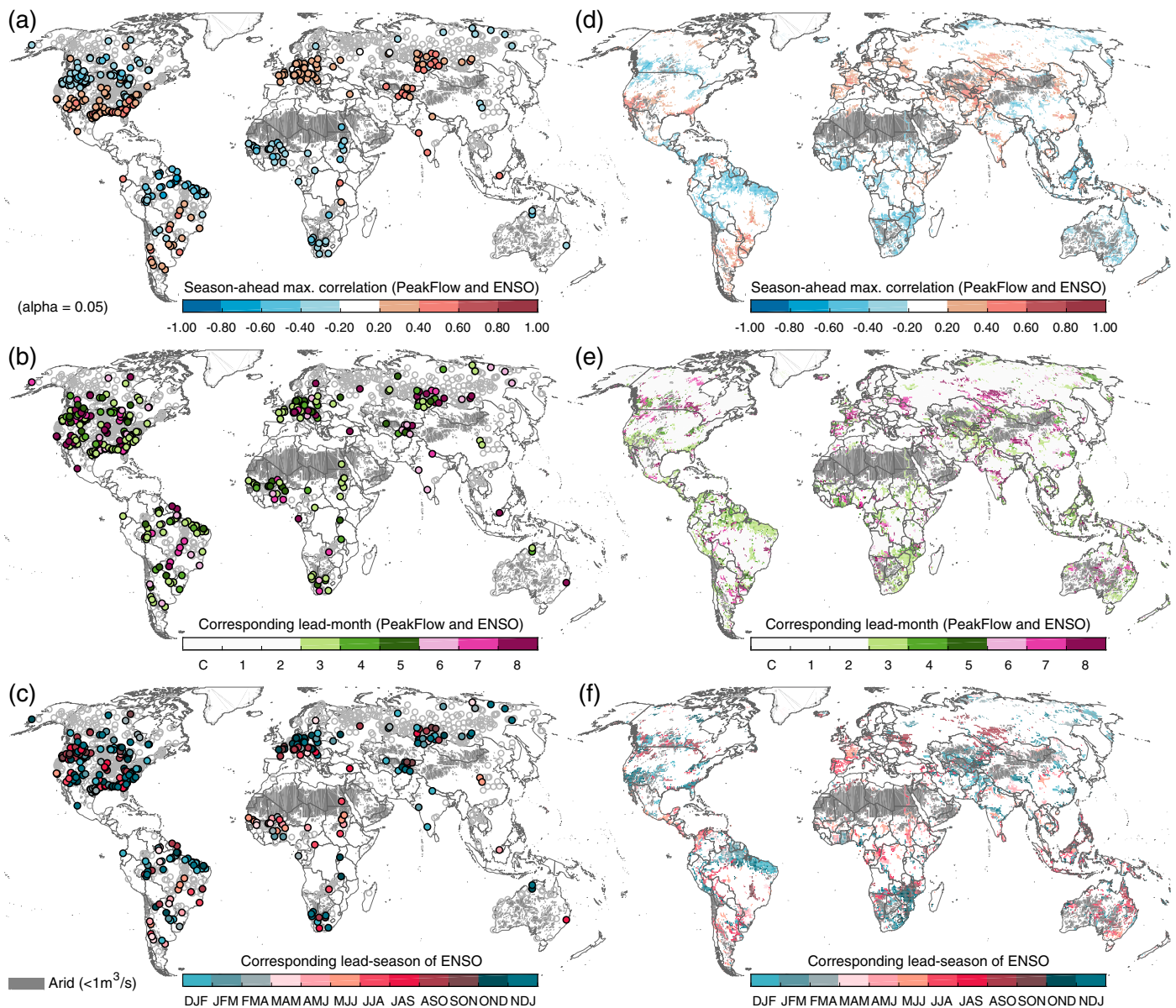


Figure 3. (a and d) Maximum lag-correlation between seasonal peak-flow and season-ahead (3–8 months) ENSO index, (b and e) corresponding lead-month of ENSO index, and (c and f) Season of ENSO index presenting the maximum correlation from the peak-flow for (a–c) observed streamflow and (d–f) simulated streamflow. Note that only stations and grid cells with statistically significant ($\alpha=0.05$) correlations during 3–8 lead-months are colored. The “C” of corresponding lead-month indicates “Concurrent.” The gray color indicates the arid areas with annual streamflow less than $1 \text{ m}^3 \text{s}^{-1}$.

correlation between ENSO and seasonal streamflow (Wanders & Wada, 2015) and ENSO and annual streamflow statistics (e.g., annual maximum) (Chiew & McMahon, 2002; Ward et al., 2010, 2014a), implying its usefulness for understanding seasonal-scale flood propensity.

The persistence of ENSO response on seasonal peak-flow is evident at many stations and grids (Figures 3b and 3c). For example, a northern-winter ENSO signal (SON-NDJ) is strongly correlated with FMA peak-flow (3–5 months later) in the northwestern, southwestern, and southeastern U.S. as well as with AMJ or MJJ peak-flow (5–8 months later) in the northern U.S. and southern Canada. The typically strong winter ENSO index is well correlated with seasonal peak-flow globally, for example, FMA peak-flow in Europe, northeastern Brazil, and northern Australia. Summertime ENSO (MJJ-JAS), often a period of development, correlates well with peak-flow in East Africa (JAS-SON) and Central America (including northern Columbia) (ASO-OND),

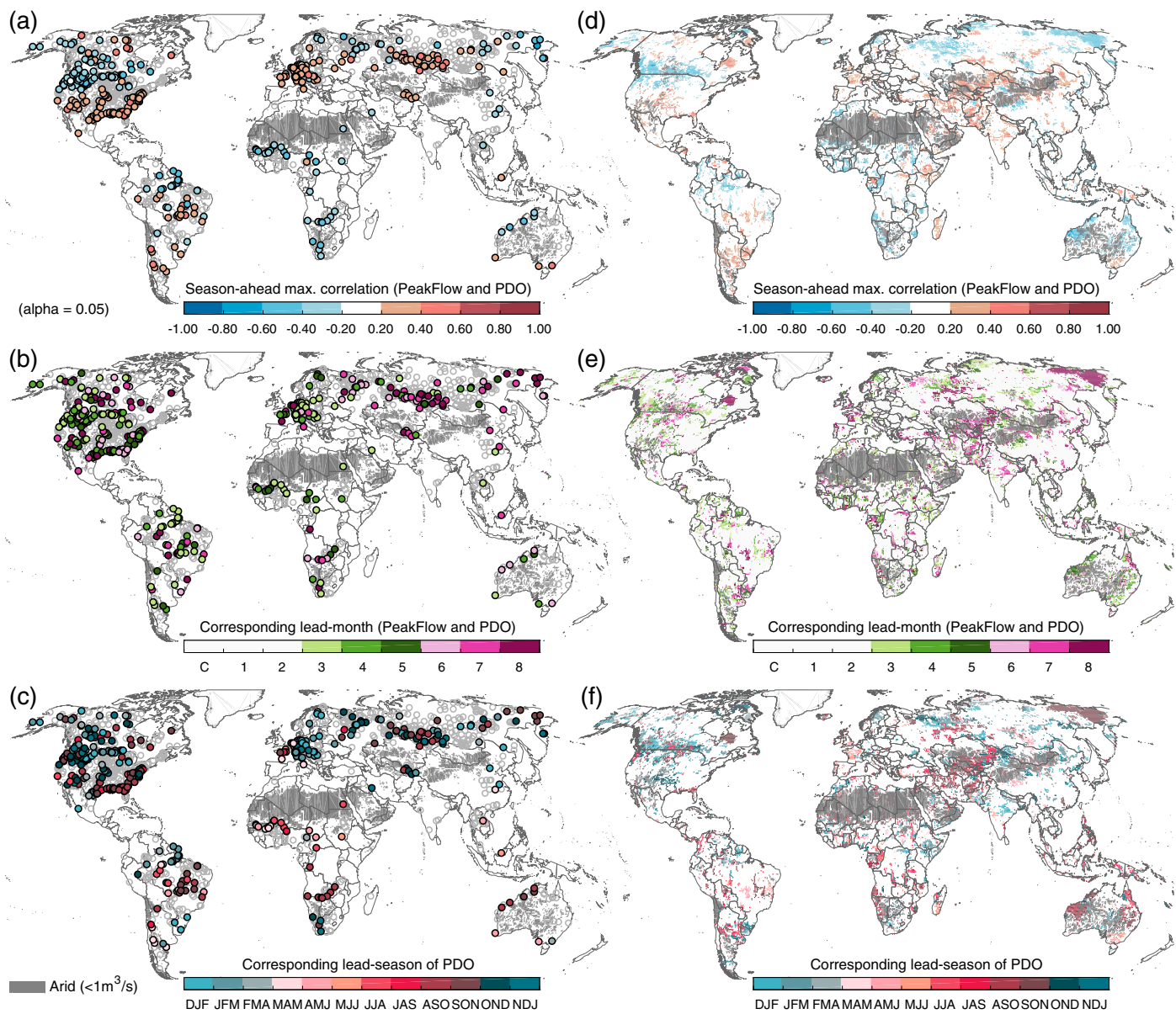


Figure 4. Same as Figure 3, but for PDO.

while the late spring ENSO index (FMA-AMJ) is strongly correlated with peak-flow in northwestern Brazil and West Africa (Figure 3).

3.1.2. PDO Influence on Seasonal Peak-Flow Globally

Like ENSO, maximum correlations between seasonal peak-flow and the season-ahead PDO index are generally similar to PDO-precipitation relationships (Mantua & Hare, 2002) (Figure 4). Also, the spatial patterns of correlations are broadly similar to those of ENSO due to PDO's ENSO-like characteristics, particularly North America and Europe (Dettinger & Diaz, 2000; Mantua & Hare, 2002; Zhang et al., 1997) (Figures 3 and 4). Temporal distinctions between PDO and ENSO, for example, include ASO-OND (OND-DJF) PDO values correlated with northern-spring peak-flow (JFM-MAM) in the southeastern U.S. (the northwestern U.S. and Europe), while the ENSO index is correlated oppositely. The exact mechanism behind the temporal differences is unclear; however, the various patterns and evolutions of North Pacific sea surface temperatures and magnitudes of low pressure systems and westerly winds in the midlatitude Pacific basin toward subtropical latitudes likely all contribute (Dettinger et al., 2001). Compared to ENSO, peak-flow is correlated

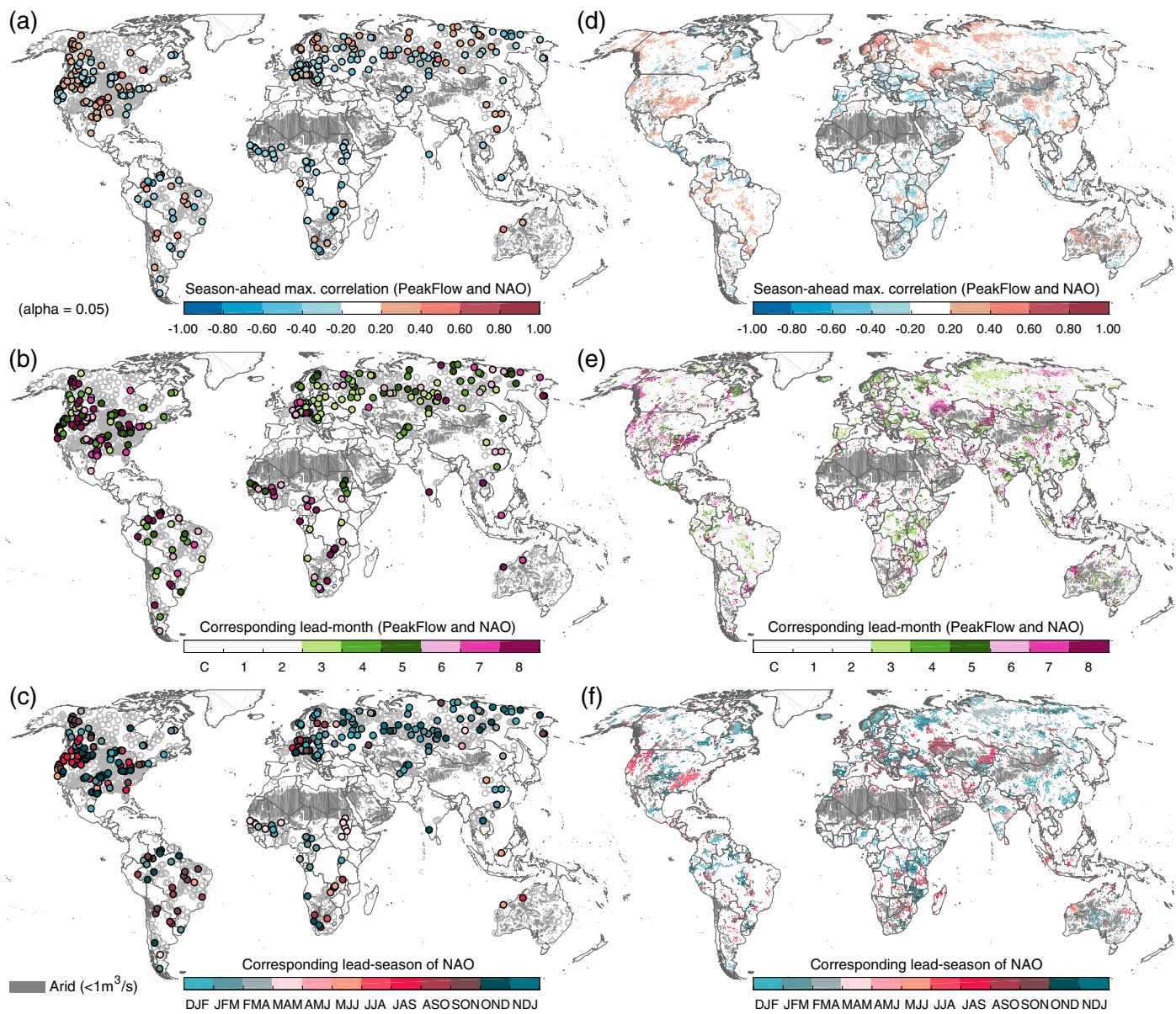


Figure 5. Same as Figure 3, but for NAO.

with PDO more broadly spatially, particularly in Africa and the northern extratropical and polar regions, in the North Pacific, and North Asia (consistent with correlation patterns represented in Dettinger and Diaz (2000)), with relatively longer leads than those demonstrated by ENSO. Impacts of PDO on seasonal peak-flow over the North Pacific are also consistent with the PDO-induced spatial pattern of seasonal precipitation and temperature anomalies (Mantua & Hare, 2002).

3.1.3. NAO Influence on Seasonal Peak-Flow Globally

NAO is strongly positively correlated with seasonal peak-flow in northern Europe, western and central Russia, the central-eastern U.S., and northwestern Canada (Figure 5). Negative correlations between seasonal peak-flow and NAO are found in central and eastern Europe, eastern North America, the west coast of the U.S., most of Africa, South Asia (Thailand), and northeastern Russia. Opposing correlation patterns between northern Europe (positive) and east-central Europe (negative) reflect the expected NAO-induced precipitation patterns (Hurrell, 1995) (Figure 5). These spatial patterns (NAO-streamflow) are also consistent with regional studies (Birsan, 2015; Hidalgo-Muñoz et al., 2015) and continental-scale studies

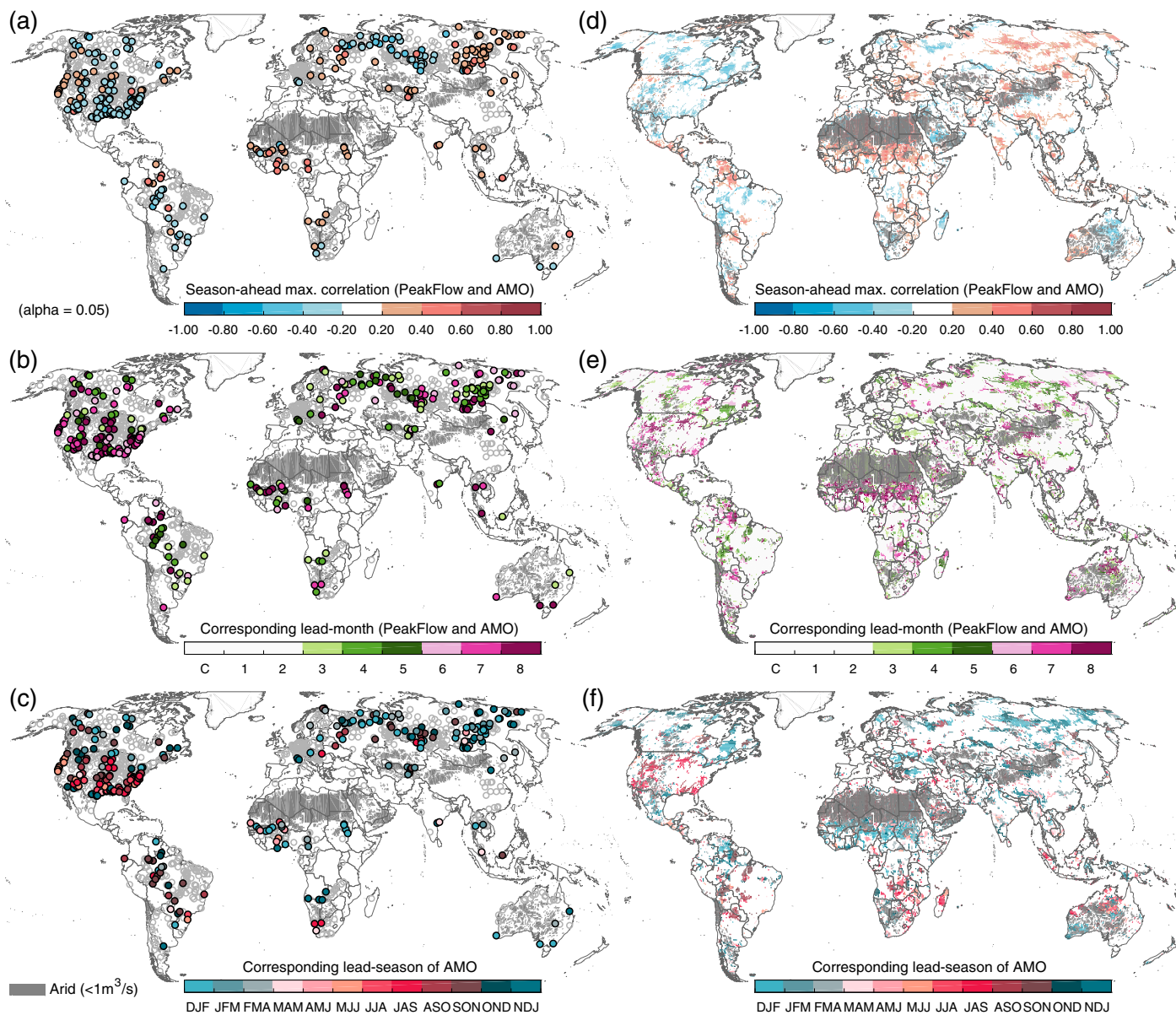


Figure 6. Same as Figure 3, but for AMO.

(Bierkens & van Beek, 2009; Bouwer et al., 2008). Although correlations vary spatially, there is a notable winter NAO (ASO-FMA) correlation with spring-summer peak-flow (JFM-MJJ) in the northern extratropic and polar regions, and significant spring NAO (JFM-MAM) correlation with JJA-OND peak-flow in tropical regions: Central America, West, Central (Sahel), and East Africa, and parts of Asia (India and China), and even southern extratropical regions (South America and southern Australia). The NAO is known to affect precipitation in southern extratropical regions at decadal timescales through the Atlantic meridional overturning circulation (Sun et al., 2015); the seasonal-scale correlations identified here in tropical and southern extratropical regions, however, may be more reflective of tropical-extratropical climate connections rather than directly linked to the North Atlantic (Dettinger & Diaz, 2000, and references therein).

3.1.4. AMO Influence on Seasonal Peak-Flow Globally

AMO is negatively correlated with seasonal peak-flow in North America, Central South America, and northwestern Russia (Figure 6). The opposite pattern in central and southeastern U.S. is consistent with the multi-decadal droughts associated with the warm (positive) AMO phase (McCabe et al., 2004). Positive

correlations are also found in Central America, northern South America (Venezuela), West and Central Africa, parts of South Asia, and central and east Russia. Peak-flow (JAS-SON) in West and Central Africa (Sahel) including the Nile River are correlated (up to 0.58) with wintertime AMO (OND-DJF) for 7–9 month lead times; this corresponds with the well-known phenomena of warm phase AMO strengthening summertime precipitation in the Sahel and West Africa (Shanahan et al., 2009; Zhang & Delworth, 2006).

3.2. Potential Predictor Identification

Statistically significantly correlated season-ahead climate drivers may be used to predict seasonal peak-flow. Not surprisingly, globally, many regions have multiple potential predictors (more than one single predictor; Figure 7 at station and grid scale). Of note, three or four of the potential predictors are simultaneously significant for central, northwestern, and southeastern U.S., central-west Canada, Central and Eastern Europe, Central Asia, northeastern Russia (Pacific), and West, East, and South Africa (Figure 7).

3.3. Streamflow Autocorrelation

As expected from literature (e.g., Chiew & McMahon, 2002), seasonal peak-flow positively correlates with lag-1 seasonal streamflow in both the observed and simulated streamflow time series (Figure 8). In many regions, this strong covariability between the season-ahead and peak season streamflow is predominantly attributable to the unclear distinction or division between seasons. For example, annual streamflow hydrographs in the western and southeastern U.S. are negatively skewed, with the peak season frequently including multiple months in the early part of the hydrograph.

Substantially high (positive) autocorrelation (>0.6) are particularly evident in regions with low seasonal streamflow variability. This often occurs in rivers with considerable base flow and a single annual streamflow peak across a long period (>3 months), such as the Amazon, Niger, and the Nile Rivers, or rivers with nearly constant streamflow (flat hydrographs), such as central Canada and Europe (Figure 8). High (positive) autocorrelation is also evident at stations downstream of large natural lakes (e.g., central Canada, Finland, and Uganda; Figure 8). The large lake systems may even dampen interannual streamflow variability (McMahon et al., 2007).

Insignificant and negative streamflow autocorrelation is evident in the north polar regions (e.g., northern Russia and western and eastern Canada; Figure 8). Typically, these areas have minimal base flow and single annual streamflow peak across a shorter period (<3 months), in stark contrast to rivers with high autocorrelation.

3.4. Season-Ahead Peak-Flow Prediction

The linear relationship between streamflow and large-scale climate patterns can vary or even be opposite across a basin. This mainly occurs in large-scale river basins with latitudinal or longitudinal shapes due to the meridional or zonal propagation of climate across the basin (Probst & Tardy, 1987). In other words, cumulative streamflow at the outlet of the basin may not represent all upstream climate impacts, producing a seeming lack of consistency of potential predictors. For example, streamflow strongly positively correlated with ENSO in the upstream reaches of the basin may not be evident in downstream sections, but instead produce an insignificant or negative correlation with ENSO. Therefore, ideally, statistical predictions for streamflow in downstream reaches of such large-scale river basins should include nonhomogeneous and cumulative climate impacts from upstream areas as well, if deemed important. This phenomenon is not addressed here; however, one could apply streamflow reconstruction techniques between downstream and upstream using nonparametric methods to identify relationships with climate drivers (Bracken et al., 2016).

In this study, we construct prediction models globally at individual stations and grids to evaluate the predictability of seasonal peak-flow, conditioned on large-scale climate drivers only (Type-A), and including streamflow autocorrelation (Type-B), separately. The percentage of stations and areas having a fair-to-good prediction ($20\% \leq \text{MSESS} \leq 0.2 \leq \text{GSS}$) for both calibration and validation data ranges according to the percentage of calibration data retained are presented in Table 1. As the percentage of calibration data applied increases, the performance of the prediction model generally decreases across the same calibration data and increases across the validation data, excepting 80% and 90% calibration data levels for Type-B predictions due to some stations with relatively short validation periods (e.g., 10% validation data for a 30 year record is only 3 years) (Table 1). When the prediction models are developed on the full data record (100% calibration data), the fair-to-good predictions globally are 16% and 15% (46% and 49%) of stations and areas, respectively, for Type-A (Type-B) predictions. Using 70% for calibration data, 9% and 8% (28% and

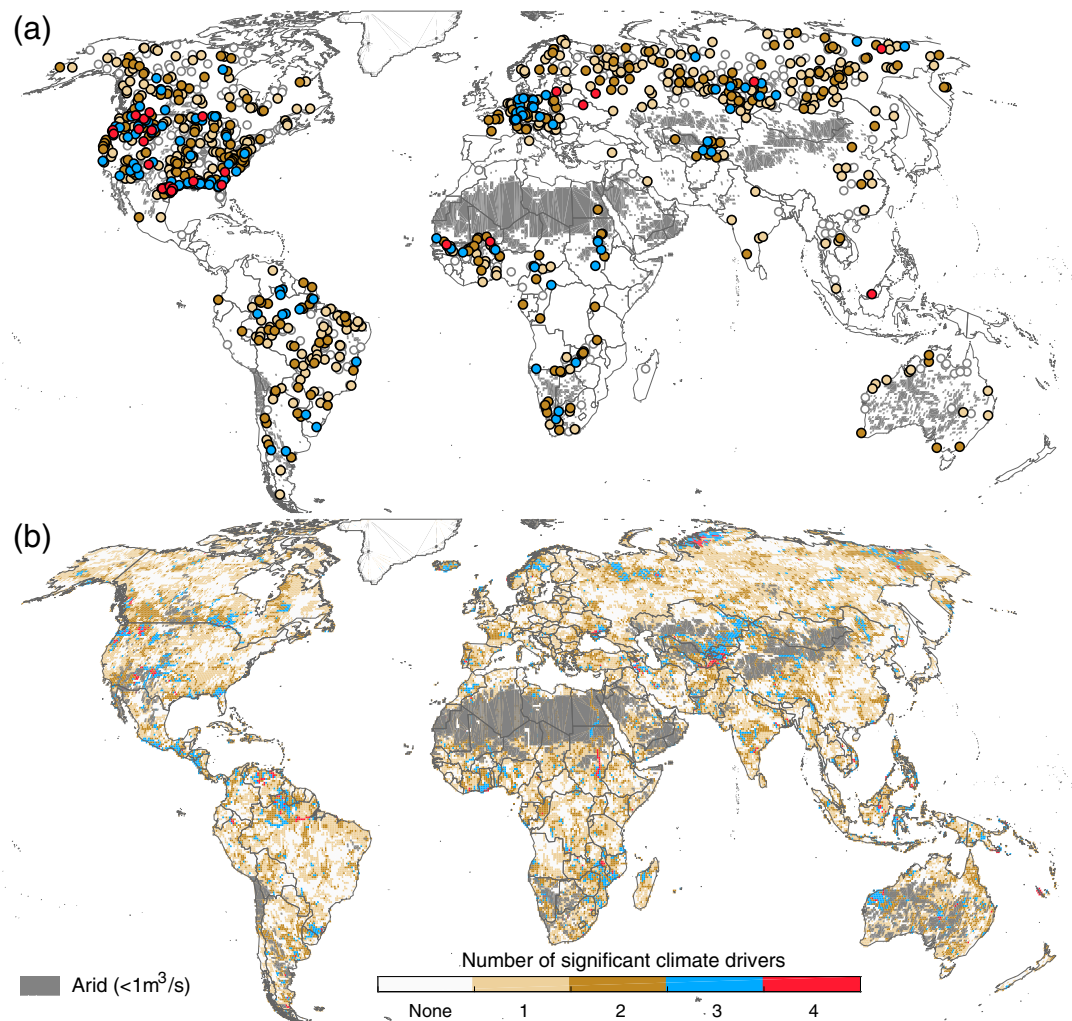


Figure 7. The number of identified predictors of climate drivers for (a) observed streamflow and (b) simulated streamflow.

29%) of stations and areas are validated as fair-to-good Type-A (Type-B) predictions (Table 1). Prediction performance is measured by correlations of skill scores (MSESS and GSS) for stations and areas having the fair-to-good prediction skill. For simulated streamflow, validation-period predictions based on 70%

Table 1
Percentage of Stations and Areas Having Fair-to-Good Prediction Performances ($20\% \leq \text{MSESS} \leq 0.2$ and $0.2 \leq \text{GSS} \leq 1.0$) According to the Percentage of Calibration Data

Calibration data (%)	Type-A				Type-B			
	Calibration		Validation		Calibration		Validation	
	Station (%)	Area (%)						
100	16.20	14.90			46.40	48.50		
90	15.90	14.10	13.20	14.00	48.30	47.10	25.60	30.70
80	18.30	15.20	10.60	10.20	49.20	47.70	25.60	30.00
70	19.40	16.00	8.60	8.30	49.80	48.30	28.30	28.60
60	21.90	16.90	7.20	6.10	48.70	48.10	28.20	26.00
50	23.20	17.50	6.80	4.30	48.90	48.60	25.40	24.60

Note. "Type-A" refers to predictions based solely on the climate predictors and "Type-B" refers to predictions based on the climate predictors and autocorrelated 1 season-ahead seasonal streamflow.

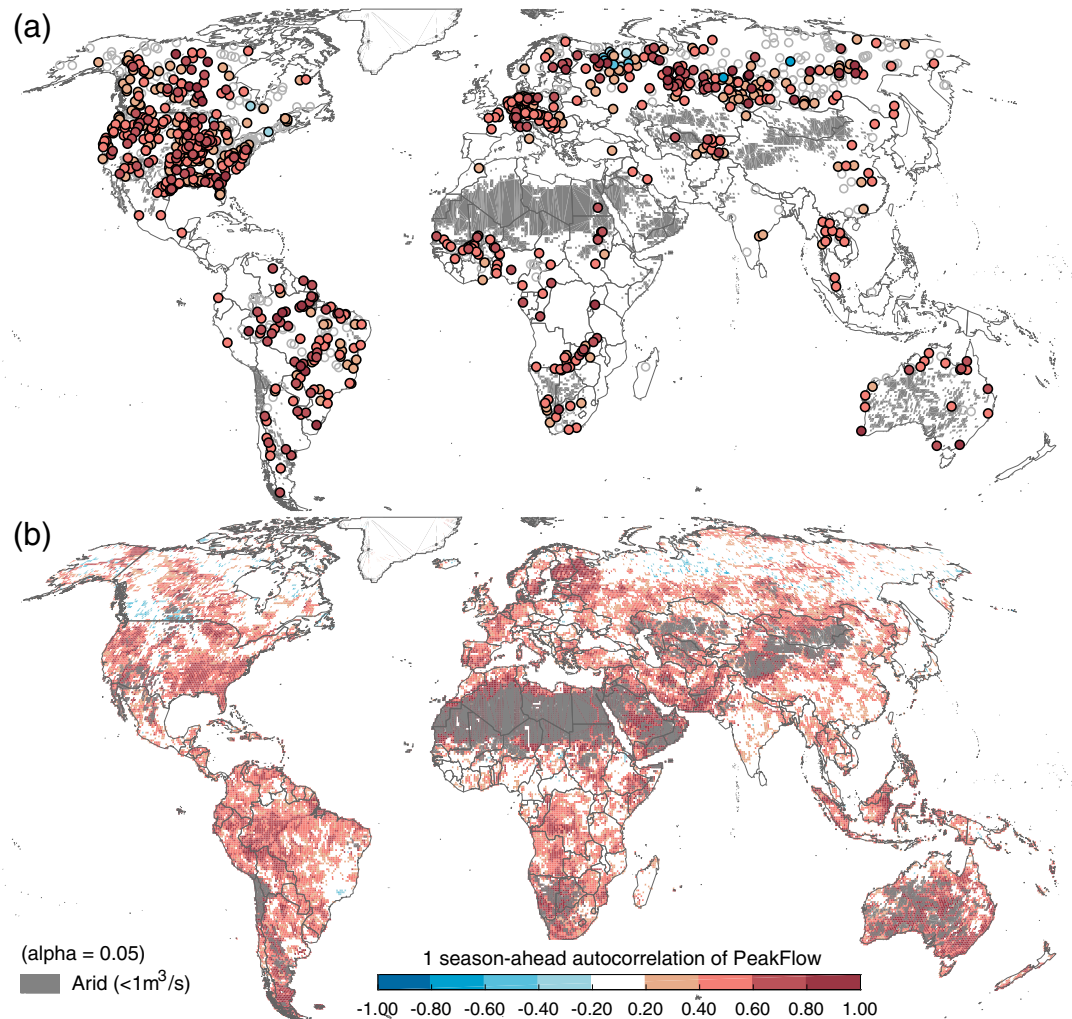


Figure 8. Autocorrelations between seasonal peak-flow and one season-ahead (3 month lead) seasonal streamflow for (a) observed streamflow and (b) simulated streamflow.

calibration data produce consistently higher correlations (0.24–0.58) than for other percentages of calibration data. For the observed streamflow, the 50% and 70% calibration data levels produce relatively higher correlations (0.19–0.50 and 0.20–0.41, respectively). Therefore, considering prediction performance and size of validation data, we select the 70% calibration data level for global prediction.

Predictions based on the 70% calibration data length are evaluated with MSESS and GSS performance metrics (Figure 9). Locations of fair and good prediction skill are also identified globally (Figure 10). In order to interpret prediction results in terms of local-scale, peak-flow predictions (Type-A and Type-B), observed streamflow are also evaluated at the selected GRDC stations (Figure 11 and Table 2). Globally, predictions conditioned on observed streamflow are nearly consistent with predictions conditioned on simulated streamflow, with both illustrating higher categorical skill score performance (GSS) compared with deterministic skill score performance (MSESS) (Figure 9). As expected, the four large-scale climate patterns do not provide consistently skillful predictions globally (Figures 9a, 9b, and 10a). However, fair predictions are found in many regions, including southwestern Canada and northwestern U.S., southwestern and southeastern U.S., the Amazon River basin, the Sahel, the Nile River, South Africa, and central and northcentral Asia (Figures 9a, 9b, and 10a).

Predictions for GRDC stations along the Suwannee River in the southeast U.S. and the Amapari River in Brazil, for example, Figures 11a and 11b and Table 2 represent a fair prediction (Type-A), and are the same as modeled simulations: ENSO, PDO, and AMO (ENSO and PDO for the Suwannee River (the Amapari River)

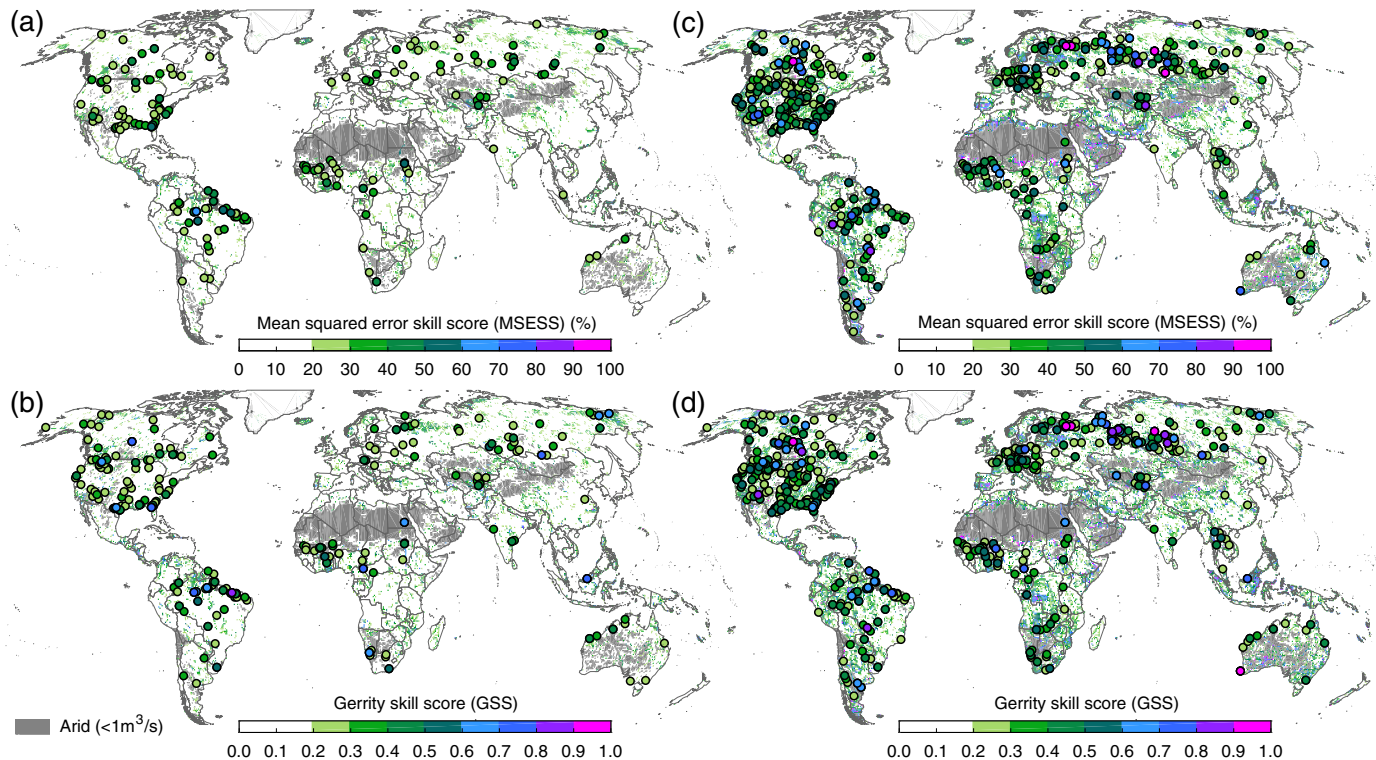


Figure 9. (a and c) The MSESS (mean squared error skill score) and (b and d) GSS (Gerrity skill score) of the seasonal peak-flow predictions based solely on the large-scale climate drivers (Type-A) (a and b) and with including the streamflow autocorrelation (Type-B) (c and d).

with nearly identical optimal lead-months (Table 1). Prediction models (at 7 and 3 month leads, respectively) perform well across the validation period, producing comparable peak-flow values and categorical flows (MESS: 57% and 46% and GSS: 0.43 and 0.25) and distributions (Figures 11a and 11b and Table 2).

It is noteworthy that fair predictions are realized in typically data-sparse regions, for example, the Niger River and Congo River basins, where seasonal peak-flow is significantly correlated with multiple predictors, particularly with AMO ($\rho = 0.22\text{--}0.59$) (Figures 6 and 7). This extends the previously demonstrated strong relationship between summertime precipitation in the Sahel and AMO (Shanahan et al., 2009; Zhang & Delworth, 2006) to include summertime peak streamflow. The station-based seasonal peak-flow in this region also illustrates an apparent linear trend or low-frequency AMO type signal, depending on the record length and period. This relationship between AMO and seasonal peak-flow is muted by the detrending process applied to remove possible spurious relationships; however with the trends retained, the seasonal peak-flow is significantly correlated with AMO ($\rho = 0.62\text{--}0.93$) in this region. Nevertheless, seasonal peak-flow prediction (Type-A) at the Niger River at Koulikord in Mali indicates a fair performance (30% MSESS and 0.25 GSS; Figure 11c). The long-term signal of AMO is not well reproduced in the streamflow simulation; however, seasonal peak-flow is well correlated with the same predictors (AMO, PDO, and ENSO) with subsequent fair prediction performances (Figure 10).

Globally, fair-to-good prediction skill is found in 8.6% (103/1,200) of stations and 8.3% of all global land surface area based on model grids where multiple predictors typically exist (Figures 7 and 10). In these regions, long-range streamflow or precipitation forecasts with nearly identical large-scale climate patterns have also been highlighted. For example, Tootle and Piechota (2004) and Nag et al. (2014) predict streamflow in the southeastern U.S. (the Suwanee River) with ENSO, Sittichok et al. (2016) use Atlantic and Pacific SSTs to predict streamflow in West Africa, and Block and Rajagopalan (2007), Funk et al. (2014), and Zhang et al. (2018) use ENSO as a main driver to forecast East African rainfall. This bolsters the utility of prediction results developed here in terms of applying good prediction skill models directly and potentially using predictors from fair prediction skill models with local predictors for modeling data-limited regions.

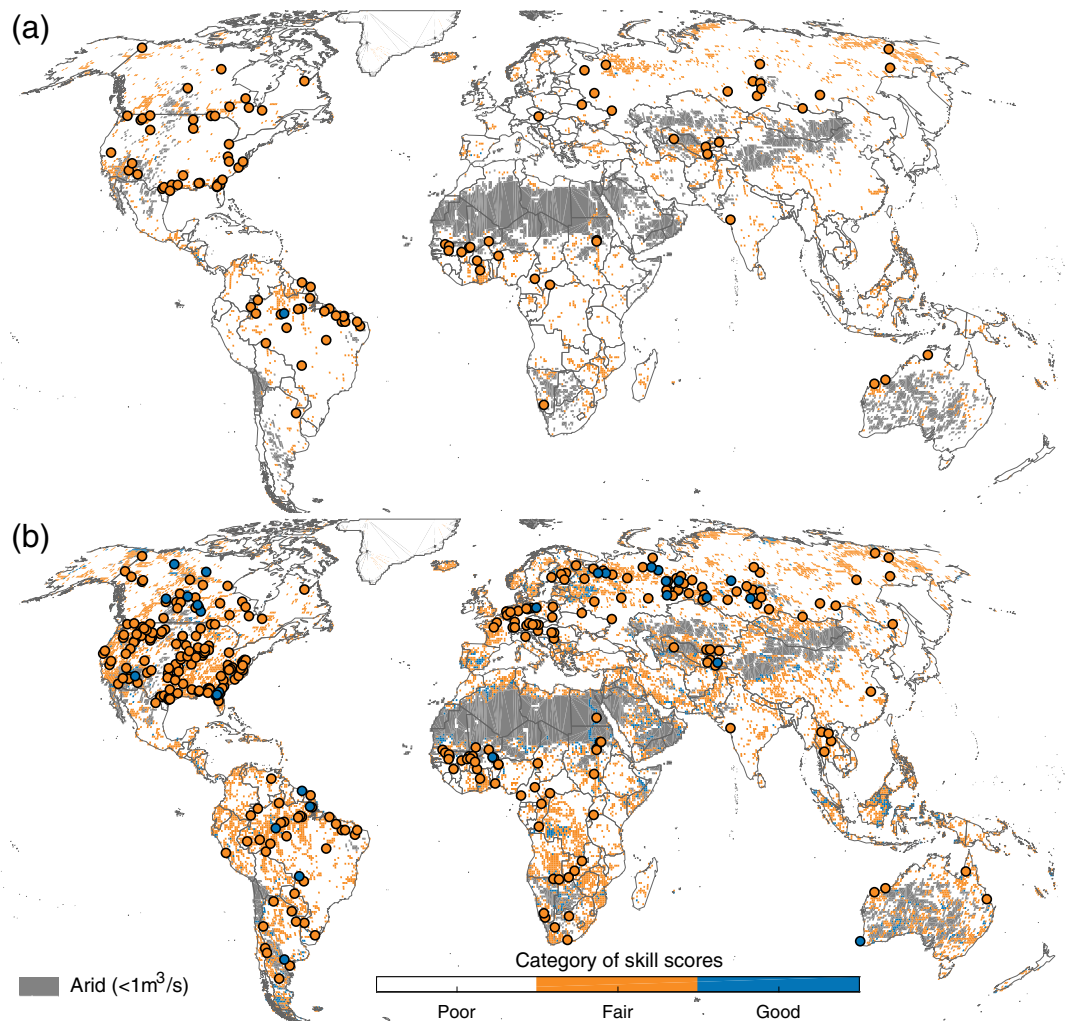


Figure 10. Identified locations with fair ($20\% \leq \text{MSESS} < 60\%$ and $0.2 \leq \text{GSS} < 0.6$) and good ($60\% \leq \text{MSESS}$ and $0.6 \leq \text{GSS}$) seasonal peak-flow prediction skill for (a) Type-A and (b) Type-B predictions. Colored circles and background colors represent predictions on streamflow stations and simulations, respectively.

When streamflow autocorrelation is included (Type-B), prediction skill increases remarkably (poor changing to fair or fair changing to good) in many regions globally in both observed and simulated streamflow, particularly in central North America, northern and southern South America, Europe, and South and East Africa (Figures 9c, 9d, and 10b). For example, the fair predictions in the Suwannee River and the Amapari River are upgraded to good predictions with changes in the regression coefficients and lead-months of climate predictors due to streamflow autocorrelation (Figure 11 and Table 2). Also, including streamflow autocorrelation, the multidecadal Sahel drought linked with the negative AMO phase during the 1960s–1990s (Zhang & Delworth, 2006) is captured remarkably well, implying potential usefulness of large-scale climate drivers and autocorrelation-based seasonal predictions for longer-term water resources management (Figure 11c and Table 2). Globally, the fair-to-good prediction skill (Type-B) is present in 28.3% (340/1,200) of stations and 28.6% of all land surface areas.

The inclusion of autocorrelation as a predictor also improves Type-A poor predictions to good predictions in many regions (e.g., central Canada and northcentral Asia) where the autocorrelation is strongly significant ($\rho = 0.8\text{--}0.9$) (e.g., lakes region) (Figures 8 and 10). The Waterhen River provides an example of the transition from poor prediction to good prediction in the lakes region; a Type-A prediction model with poor performance (6% MSESS and 0.05 GSS) is developed with ENSO as the only predictor; however, including streamflow autocorrelation ($\rho = 0.82$), a Type-B prediction model produces a good performance (77%

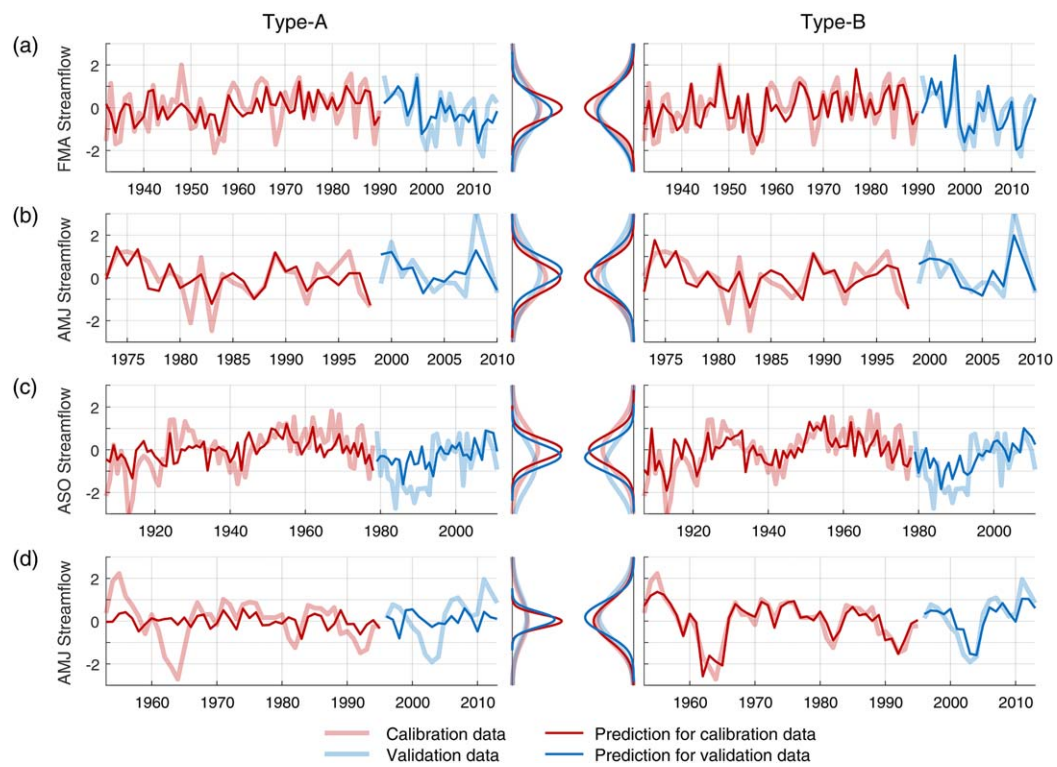


Figure 11. Season-ahead global peak-flow predictions at the selected GRDC stations and its normal distributions at (a) the Suwannee River at Branford, U.S., (GRDC 4149780), (b) the Amapari River at Serra do Navio, Brazil (GRDC 3631060), (c) the The Niger River at Koulikoro, Mali (GRDC 1134100), and (d) the Waterhen River near Waterhen, Canada (GRDC 4213603). The plots of annual time series of normalized log-transformed peak-flows and their normal PDF lines on the left and right indicate predictions based solely on potential climatic drivers (Type-A) and with streamflow autocorrelation (Type-B), respectively. The PDF lines of predictions including autocorrelation (right) are flipped horizontally with the same scales to the left for easy comparison.

MSESS and 0.85 GSS) (Figure 11d and Table 2). The magnitude of the regression coefficient for one season-ahead streamflow (0.88) is clearly higher than ENSO (-0.15) indicating that considerable amount of the seasonal peak-flow variance is attributable to autocorrelation in the model (Table 2). Although streamflow

Table 2
Season-Ahead Global Peak-Flow Prediction at the Selected Locations (Same With Figure 11)

Station	Predictors	Type	PCR Models with optimal lead-months	Period	MSESS (%)	GSS	Prediction
(a) The Suwannee River at Branford, U.S. GRDC 4149780	ENSO PDO AMO	A	$y_t = 0.352 \text{ ENSO}_{t-7} + 0.222 \text{ PDO}_{t-8} - 0.368 \text{ AMO}_{t-8}$	Calibration	31	0.32	Fair
		B	$y_t = 0.584 y_{t-3} + 0.236 \text{ ENSO}_{t-7} + 0.192 \text{ PDO}_{t-7} - 0.220 \text{ AMO}_{t-7}$	Validation	57	0.43	Fair
(b) The Amapari River at Serra do Navio, Brazil. GRDC 3631060	ENSO PDO	A	$y_t = -0.421 \text{ ENSO}_{t-3} - 0.421 \text{ PDO}_{t-3}$	Calibration	61	0.52	Fair
		B	$y_t = 0.349 y_{t-3} - 0.363 \text{ ENSO}_{t-5} + 0.171 \text{ PDO}_{t-7}$	Validation	65	0.66	Good
(c) The Niger River at Koulikoro, Mali. GRDC 1134100	PDO NAO AMO	A	$y_t = -0.376 \text{ PDO}_{t-5} - 0.239 \text{ NAO}_{t-5} + 0.236 \text{ AMO}_{t-5}$	Calibration	27	0.31	Fair
		B	$y_t = 0.431 y_{t-3} - 0.334 \text{ PDO}_{t-4} - 0.304 \text{ NAO}_{t-5} + 0.191 \text{ AMO}_{t-8}$	Validation	30	0.25	Fair
(d) The Waterhen River near Waterhen, Canada. GRDC 4213603	ENSO	A	$y_t = -0.311 \text{ ENSO}_{t-3}$	Calibration	48	0.34	Fair
		B	$y_t = 0.881 y_{t-3} - 0.156 \text{ ENSO}_{t-5}$	Validation	45	0.37	Fair
				Calibration	10	0.09	Poor
				Validation	6	0.05	Poor
				Calibration	84	0.72	Good
				Validation	77	0.85	Good

Note. The y_t indicates normalized log-transformed seasonal streamflow (y) in the predefined peak season (t), and Index_{t-k} means climate index at k lead-month ahead of the peak season (t). The y_{t-3} refers one season (3 month) ahead seasonal streamflow to the seasonal peak-flow (y_t).

autocorrelation generally enhances the Type-A prediction performance globally, in some locations prediction performance is reduced (e.g., a station with fair Type-A and poor Type-B predictions in northern Australia) (Figure 10), implying that the inclusion of autocorrelation in the prediction models does not always necessitate enhanced performance, and each case needs to be considered independently.

Occurrences of poor prediction skill ($MSESS < 20\%$ or $GSS < 0.2$), inferior to or only moderately better than a climatological mean forecast, are found in both types of predictions, and typically with a single predictor (Figures 7 and 10). Although we found significant streamflow autocorrelation globally (Figure 8), the Type-B model with a single autocorrelation predictor typically predicts relatively constant peak-flow values compared to observed or simulated streamflow and produces higher squared errors than climatological means. This case is often found at locations having low mean peak-flow with multiple peaks, resulting in biased categorical predictions compared to those of observed or simulated streamflow. In contrast, poor GSS cases also occur for predictions of exceptional peaks compared to the streamflow observations or simulations. Here we simply apply one season-ahead autocorrelation as a potential predictor to the linear model; however, higher-order autoregressive models could be further applied to gauge model improvement.

Seasonal peak-flow prediction on stations with an “allowable” regulation category represent higher performance than those of stations with a “none” regulation category; fair-to-good Type-B prediction performance results for 32% (26%) of stations with allowable (none) regulation. This implies usefulness of the identified climate-driven relationship and prediction models in the acceptably regulated regions.

Numerous limitations may be worth investigating in future studies. Although the regression coefficients of potential climate predictors may account for coupled climate impacts on peak-flow at the seasonal scale, it is subjective to the data included in the model. To account for coupled climate impacts, additional objective analysis (e.g., categorical significance tests with different phases of climate drivers) are required prior to model development, including decadal and multidecadal climatic patterns linked to interannual climate patterns (e.g., ENSO) (Enfield et al., 2001; García-garcía & Ummenhofer, 2015; Livezey & Smith, 1999; McCabe et al., 2004; Tootle et al., 2005). In addition, various prediction models specifically able to handle coupled climate impacts (e.g., Bayesian or categorical prediction model) could be tested and compared for model selection. Improved (nonlinear or nonparametric) statistical prediction models could be applied to test the possibility of improving predictability. Relatively short streamflow records may not be sufficient to account for long-term (e.g., multidecadal) variations or include a significant number of climate events (e.g., El Niños or La Niñas). This may occur at stations with relatively short records or even for streamflow simulations given the decision to calibrate the prediction model with 70% of the data. Longer streamflow records and centennial streamflow simulations may be justified for further studies. Although seasonal peak-flow provides a 3 month average tendency as induced by season-ahead climate drivers, one can disaggregate to monthly and daily timescale to evaluate specific flood propensities using stochastic temporal disaggregation techniques (Prairie et al., 2007).

In seasonal climate and streamflow predictions, initial conditions often play a pivotal role (Clove & Pappenberger, 2009; Shukla & Lettenmaier, 2011). A one season-ahead streamflow Type-B prediction may contain direct (e.g., peak-flow) or indirect (e.g., base flow) initial conditions; however, other season-ahead initial conditions (e.g., snow accumulation, soil moisture, evaporation, etc.) could provide further predictability of seasonal peak-flow in particular basins (e.g., snow-fed basins or arid regions), even where a significant autocorrelation does not exist. The identified relationships between climate drivers and seasonal peak-flow represent generally similar patterns with those of climate drivers and precipitation reported in literature; however, distinct patterns are also identified in some locations. Potential reasons that may explain these distinct patterns include lagged snowmelt impacts over highland areas feeding peak-flow in spring/summer seasons when the precipitation may not be strongly coupled with a climate driver, and integration of cumulative hydrological processes diminishing or enhancing the precipitation-climate driver relationship across river basins. Finally, streamflow simulations from other global hydrological models could be compared and validated to boost confidence for predictions in data-scarce regions.

4. Conclusions

In this study, we attribute covariability of seasonal peak-flow to season-ahead (3–8 month lead times) large-scale climate patterns (ENSO, PDO, NAO, and AMO) and autocorrelation globally and use these relationships

to construct and evaluate season-ahead prediction models. By obtaining extensive streamflow observations (GRDC and HCDN) and screening regulated stations, we retain numerous spatially unbiased stations with long-term records globally. Using the global streamflow simulations from PCR-GLOBWB, we identify the impacts of individual climate patterns on seasonal peak-flow, even in data-limited regions globally. This builds on previous studies focused on regional or continental impacts only, and typically addressing annual streamflow statistics for evaluating a mean tendency only, rather than evaluating seasonal peak-flow that may lead to estimates of seasonal flood propensity. We develop season-ahead seasonal peak-flow prediction models globally using the optimal lead-months selected by the LOOCV and the PCR model for each station and grid; predictability is evaluated by MSESS and GSS. Results described in section 3 lead to the following conclusions:

1. We find significant relationships between seasonal peak-flow and season-ahead large-scale climate drivers globally using both streamflow observations and simulations (Figures 3–6). The identified patterns are generally consistent with the climate driver-induced anomalous precipitation patterns. However, stronger or weaker relationships are also found in large-scale river basins due to the cumulatively enhanced or reduced impacts. Statistically significant climate patterns are typically associated with the characteristics of both seasonal streamflow and annual maximum flow, providing relationships tailored to seasonal-scale flood propensity. The persistence of season-ahead climate signals is also identified globally (Figures 3–6), which could improve the understanding of impacts of noticeable climate signals (e.g., winter ENSO) on seasonal peak-flow. Globally, multiple potential predictors are found in many regions (Figure 7).
2. Seasonal peak-flow positively correlates with lag-1 season-ahead seasonal streamflow in many regions, indicating high autocorrelation (Figure 8). Substantially high (positive) serial correlations (>0.6) are found in areas having low seasonal variability with considerable base flow and single annual peaks across a relatively long period (>3 months) or in areas with constant annual streamflow. Highly positive correlations with low seasonal variability are also found in observed streamflow downstream of large lakes systems.
3. Although this study uses only four large-scale climate patterns and autocorrelation, fair-to-good prediction skill ($20\% \leq \text{MSESS}$ and $0.2 \leq \text{GSS}$) for seasonal peak-flow are found in many climate-sensitive regions globally (28% of stations and 29% of land area) (Figure 10). By including autocorrelation, prediction skill increases remarkably in many regions globally (although clearly not all) for both observed and simulated streamflow in central North America, northern and western South America, Europe, and South and East Africa. Particularly, in western and central Africa where the AMO significantly affects summer precipitation, models well predict the long-term trend of seasonal peak-flow. Remarkably, good prediction skill ($60\% \leq \text{MSESS}$ and $0.6 \leq \text{GSS}$) is also presented in numerous regions, such as central Canada, southeastern U.S., northeastern South America, and northcentral Asia.

The covariability between large-scale climate and seasonal peak-flow that leads to prediction models with fair performance may provide the groundwork for local-scale seasonal peak-flow prediction by coupling relevant global-scale climate patterns with local climatic (e.g., regional monsoon system) and hydrological (e.g., soil moisture) predictors. Prediction models with good performance at one season leads can complement operational climate-informed ensemble streamflow forecasts (e.g., weighted multimodel ensemble forecasts) (van Dijk et al., 2013; Werner et al., 2004) which provide hydrological information at relatively short lead times (e.g., days to weeks). Additionally, predictions with a good performance can provide practical information for long-range flood preparedness and water resources management (e.g., humanitarian actions; forecast-based financing, and emergency actions) (Coughlan de Perez et al., 2015). Finally, the approach developed here may be especially attractive in regions with limited observations and/or little capacity to develop early warning systems, particularly at long-leads.

Acknowledgments

We thank the GRDC for providing streamflow observations. The GRDC streamflow data are freely available on request (http://www.bafg.de/GRDC/EN/Home/homepage_node.html). The PCR-GLOBWB simulation data used in this study and Ward et al. (2013) are originally obtained from Utrecht University and available on request (<http://www.earthsurfacehydrology.nl/>). Funding for D.L. was provided by Global Health Institute and the Graduate School of the University of Wisconsin-Madison. P.J.W. received funding from the Netherlands Organisation for Scientific Research (NWO) in the form of a VIDI grant (grant 016.161.324). We also thank the editor and three anonymous reviewers for their valuable comments and suggestions.

References

- Alfieri, L., Burek, P., Dutra, E., Krzeminski, B., Muraro, D., Thielen, J., et al. (2013). GloFAS—Global ensemble streamflow forecasting and flood early warning. *Hydrology and Earth System Sciences*, 17(3), 1161–1175. <https://doi.org/10.5194/hess-17-1161-2013>
- Bierkens, M. F. P., & van Beek, L. P. H. (2009). Seasonal predictability of European Discharge: NAO and hydrological response time. *Journal of Hydrometeorology*, 10(4), 953–968. <https://doi.org/10.1175/2009JHM1034.1>
- Birsan, M.-V. (2015). Trends in monthly natural streamflow in Romania and linkages to atmospheric circulation in the North Atlantic. *Water Resource Management*, 29(9), 3305–3313. <https://doi.org/10.1007/s11269-015-0999-6>
- Block, P., & Rajagopalan, B. (2007). Interannual variability and ensemble forecast of upper Blue Nile basin Kiremt season precipitation. *Journal of Hydrometeorology*, 8(3), 327–343. <https://doi.org/10.1175/JHM580.1>

- Bouwer, L. M., Vermaat, J. E., & Aerts, J. C. J. H. (2008). Regional sensitivities of mean and peak river discharge to climate variability in Europe. *Journal of Geophysical Research*, 113, D19103. <https://doi.org/10.1029/2008JD010301>
- Bracken, C., Rajagopalan, B., & Woodhouse, C. (2016). A Bayesian hierarchical nonhomogeneous hidden Markov model for multisite streamflow reconstructions. *Water Resources Research*, 52, 7837–7850. <https://doi.org/10.1002/2016WR018887>.
- Burn, D. H., & Arnell, N. W. (1993). Synchronicity in global flood responses. *Journal of Hydrology*, 144(1–4), 381–404. [https://doi.org/10.1016/0022-1694\(93\)90181-8](https://doi.org/10.1016/0022-1694(93)90181-8)
- Cayan, D. R., Redmond, K. T., & Riddle, L. G. (1999). ENSO and hydrologic extremes in the Western United States*. *Journal of Climate*, 12(9), 2881–2893. [https://doi.org/10.1175/1520-0442\(1999\)012<2881:EAHEIT>2.0.CO;2](https://doi.org/10.1175/1520-0442(1999)012<2881:EAHEIT>2.0.CO;2)
- Chiew, F. H. S., & McMahon, T. A. (2002). Global ENSO-streamflow teleconnection, streamflow forecasting and interannual variability. *Hydrological Sciences Journal*, 47(3), 505–522. <https://doi.org/10.1080/02626660209492950>
- Chiew, F. H. S., Zhou, S. L., & McMahon, T. A. (2003). Use of seasonal streamflow forecasts in water resources management. *Journal of Hydrology*, 270(1–2), 135–144. [https://doi.org/10.1016/S0022-1694\(02\)00292-5](https://doi.org/10.1016/S0022-1694(02)00292-5)
- Croke, H. L., & Pappenberger, F. (2009). Ensemble flood forecasting: A review. *Journal of Hydrology*, 375(3–4), 613–626. <https://doi.org/10.1016/j.jhydrol.2009.06.005>
- Coughlan de Perez, E., van den Hurk, B., van Aalst, M. K., Jongman, B., Klose, T., & Suarez, P. (2015). Forecast-based financing: An approach for catalyzing humanitarian action based on extreme weather and climate forecasts. *Natural Hazards and Earth System Sciences*, 15(4), 895–904. <https://doi.org/10.5194/nhess-15-895-2015>
- Dai, A., & Wigley, T. M. L. (2000). Global patterns of ENSO-induced precipitation. *Geophysical Research Letters*, 27(9), 1283–1286. <https://doi.org/10.1029/1999GL011140>
- Demargne, J., Wu, L., Regonda, S. K., Brown, J. D., Lee, H., He, M., et al. (2014). The science of NOAA's operational hydrologic ensemble forecast service. *Bulletin of the American Meteorological Society*, 95(1), 79–98. <https://doi.org/10.1175/BAMS-D-12-00081.1>
- Dettinger, M. D., Battisti, D. S., Garreaud, R. D., McCabe, G., & Bitz, C. M. (2001). Interhemispheric effects of interannual and decadal ENSO-like climate variations on the Americas. *Interhemispheric Climate Linkages*, 1–16.
- Dettinger, M. D., Cayan, D. R., McCabe, G. J., & Marengo, J. A. (2000). Multiscale streamflow variability associated with El Niño/Southern Oscillation. In H. F. Diaz & V. Markgraf (Eds.), *El Niño and the Southern Oscillation: Multiscale variability and global and regional impacts* (pp. 113–146). Cambridge, UK: Cambridge University Press.
- Dettinger, M. D., & Diaz, H. F. (2000). Global characteristics of stream flow seasonality and variability. *Journal of Hydrometeorology*, 1(4), 289–310. [https://doi.org/10.1175/1525-7541\(2000\)001<0289:GCOSFS>2.0.CO;2](https://doi.org/10.1175/1525-7541(2000)001<0289:GCOSFS>2.0.CO;2)
- Doblas-Reyes, F. J., García-Serrano, J., Liepert, F., Biescas, A. P., & Rodrigues, L. R. L. (2013). Seasonal climate predictability and forecasting: Status and prospects. *Wiley Interdisciplinary Reviews: Climate Change*, 4(4), 245–268. <https://doi.org/10.1002/wcc.217>
- Döll, P., & Lehner, B. (2002). Validation of a new global 30-min drainage direction map. *Journal of Hydrology*, 258(1–4), 214–231. [https://doi.org/10.1016/S0022-1694\(01\)00565-0](https://doi.org/10.1016/S0022-1694(01)00565-0)
- Doocy, S., Daniels, A., Murray, S., & Kirsch, T. D. (2013). The human impact of floods: A historical review of events 1980–2009 and systematic literature review. *PLOS Currents*, 5, 1–27. <https://doi.org/10.1371/currents.dis.f4deb457904936b07c09daa98ee8171a>
- Emerton, R., Croke, H. L., Stephens, E. M., Zsoter, E., Woolnough, S. J., & Pappenberger, F. (2017). Complex picture for likelihood of ENSO-driven flood hazard. *Nature Communications*, 8, 14796. <https://doi.org/10.1038/ncomms14796>
- Emerton, R. E., Stephens, E. M., Pappenberger, F., Pagano, T. C., Weerts, A. H., Wood, A. W., et al. (2016). Continental and global scale flood forecasting systems. *Wiley Interdisciplinary Reviews: Water*, 3, 391–418. <https://doi.org/10.1002/wat2.1137>
- Enfield, D. B., Mestas-Nuñez, A. M., & Trimble, P. J. (2001). The Atlantic multidecadal oscillation and its relation to rainfall and river flows in the continental U.S. *Geophysical Research Letters*, 28(10), 2077–2080. <https://doi.org/10.1029/2000GL012745>
- Funk, C., Hoell, A., Shukla, S., Bladé, I., Liebmann, B., Roberts, J. B., et al. (2014). Predicting East African spring droughts using Pacific and Indian Ocean sea surface temperature indices. *Hydrology and Earth System Sciences*, 18(12), 4965–4978. <https://doi.org/10.5194/hess-18-4965-2014>
- Gandin, L. S., & Murphy, A. H. (1992). Equitable skill scores for categorical forecasts. *Monthly Weather Review*, 120(2), 361–370. [https://doi.org/10.1175/1520-0493\(1992\)120<0361:ESSFCF>2.0.CO;2](https://doi.org/10.1175/1520-0493(1992)120<0361:ESSFCF>2.0.CO;2)
- García-García, D., & Ummenhofer, C. C. (2015). Multidecadal variability of the continental precipitation annual amplitude driven by AMO and ENSO. *Geophysical Research Letters*, 42, 526–535. <https://doi.org/10.1002/2014GL062451>
- Gerrity, J. P. (1992). A note on Gandin and Murphy's equitable skill score. *Monthly Weather Review*, 120(11), 2709–2712. [https://doi.org/10.1175/1520-0493\(1992\)120<2709:ANOGAM>2.0.CO;2](https://doi.org/10.1175/1520-0493(1992)120<2709:ANOGAM>2.0.CO;2)
- Global Runoff Data Centre (2007). *Major river basins of the World/Global Runoff Data Centre*. GRDC, Koblenz, Germany: Federal Institute of Hydrology (BfG).
- Golnaragh, M., Douris, J., & Migraine, J.-B. (2009). *Saving lives through early warning systems and emergency preparedness*. Tudor House, Leicester: Tudor Rose.
- Hidalgo-Muñoz, J. M., Gámiz-Fortis, S. R., Castro-Díez, Y., Argüeso, D., & Esteban-Parra, M. J. (2015). Long-range seasonal streamflow forecasting over the Iberian Peninsula using large-scale atmospheric and oceanic information. *Water Resources Research*, 51, 3543–3567. <https://doi.org/10.1002/2014WR016826>
- Hurrell, J. W. (1995). Decadal trends in the north Atlantic oscillation: Regional temperatures and precipitation. *Science*, 269(5224), 676–679. <https://doi.org/10.1126/science.269.5224.676>
- Hurrell, J. W., & Deser, C. (2009). North Atlantic climate variability: The role of the North Atlantic Oscillation. *Journal of Marine Systems*, 78(1), 28–41. <https://doi.org/10.1016/j.jmarsys.2008.11.026>
- International Commission on Large Dams (ICOLD) (2009). *World register of dams. Version updates 1998–2009*. Paris: ICOLD.
- IFRC (2011). *The Red Cross Red Crescent approach to disaster and crisis management*. Geneva: IFRC.
- Jolliffe, I. T. (2002). *Principal component analysis*. Springer Series in Statistics. New York, NY: Springer.
- Jolliffe, I. T., & Stephenson, D. B. (2012). *Forecast verification: A practitioner's guide in atmospheric science*. Hoboken, NJ: John Wiley.
- Knight, J. R., Folland, C. K., & Scaife, A. A. (2006). Climate impacts of the Atlantic multidecadal oscillation. *Geophysical Research Letters*, 33, L17706. <https://doi.org/10.1029/2006GL026242>
- Lee, D., Ward, P., & Block, P. (2015). Defining high-flow seasons using temporal streamflow patterns from a global model. *Hydrology and Earth System Sciences*, 19(11), 4689–4705. <https://doi.org/10.5194/hess-19-4689-2015>
- Lehner, B., Liermann, C. R., Revenga, C., Vörösmarty, C., Fekete, B., Crouzet, P., et al. (2011). High-resolution mapping of the world's reservoirs and dams for sustainable river-flow management. *Frontiers in Ecology and the Environment*, 9(9), 494–502. <https://doi.org/10.1890/100125>
- Lehner, B., Verdin, K., & Jarvis, A. (2008). New global hydrography derived from spaceborne elevation data. *Eos, Transactions, American Geophysical Union*, 89(10), 93. <https://doi.org/10.1029/2008EO100001>

- Liang, Y.-C., Chou, C.-C., Yu, J.-Y., & Lo, M.-H. (2016). Mapping the locations of asymmetric and symmetric discharge responses in global rivers to the two types of El Niño. *Environmental Research Letters*, 11(4), 44012. <https://doi.org/10.1088/1748-9326/11/4/044012>
- Lins, H. F. (2012). *USGS Hydro-Climatic Data Network 2009 (HCDN-2009): U.S. Geological Survey Fact Sheet 2012-3047* (4 p.). Reston, VA: U.S. Geological Survey.
- Livezey, R. E., & Smith, T. M. (1999). Covariability of aspects of North American Climate with global sea surface temperatures on interannual to interdecadal timescales. *Journal of Climate*, 12(1), 289–302. <https://doi.org/10.1175/1520-0442-12.1.289>
- Mantua, N. J., & Hare, S. R. (2002). The Pacific decadal oscillation. *Journal of Oceanography*, 58(1), 35–44. <https://doi.org/10.1023/A:1015820616384>
- Mason, S. J., & Goddard, L. (2001). Probabilistic precipitation anomalies associated with ENSO. *Bulletin of the American Meteorological Society*, 82(4), 619–638. [https://doi.org/10.1175/1520-0477\(2001\)082<0619:PAAWE>2.3.CO;2](https://doi.org/10.1175/1520-0477(2001)082<0619:PAAWE>2.3.CO;2)
- McCabe, G. J., Palecki, M. A., & Betancourt, J. L. (2004). Pacific and Atlantic Ocean influences on multidecadal drought frequency in the United States. *Proceedings of the National Academy of Sciences of the United States of America*, 101(12), 4136–4141. <https://doi.org/10.1073/pnas.0306738101>
- McCabe, G. J., & Wolock, D. M. (2008). Joint variability of global runoff and global sea surface temperatures. *Journal of Hydrometeorology*, 9(4), 816–824. <https://doi.org/10.1175/2008JHM943.1>
- McMahon, T. A., Peel, M. C., Vogel, R. M., & Pegram, G. G. S. (2007). Global streamflows—Part 3: Country and climate zone characteristics. *Journal of Hydrology*, 347(3–4), 272–291. <https://doi.org/10.1016/j.jhydrol.2007.09.013>
- Messager, M. L., Lehner, B., Grill, G., Nedeva, I., & Schmitt, O. (2016). Estimating the volume and age of water stored in global lakes using a geo-statistical approach. *Nature Communications*, 7, 13603. <https://doi.org/10.1038/ncomms13603>
- Munich Re. (2012). *Topics geo 2012 issue. Natural catastrophes 2011. Analyses, assessments, positions*. Munich: Münchener Rückversicherungs-Gesellschaft.
- Nag, B., Misra, V., & Bastola, S. (2014). Validating ENSO teleconnections on Southeastern U.S. winter hydrology. *Earth Interactions*, 18(15), 1–23. <https://doi.org/10.1175/EL-D-14-0007.1>
- Palmer, T. N. (2000). Predicting uncertainty in forecasts of weather and climate. *Reports on Progress in Physics*, 63(2), 71–116. <https://doi.org/10.1088/0034-4885/63/2/201>
- Piechota, T. C., Chiew, F. H. S., Dracup, J. A., & McMahon, T. A. (1998). Seasonal streamflow forecasting in eastern Australia and the El Niño–Southern Oscillation. *Water Resources Research*, 34(11), 3035–3044. <https://doi.org/10.1029/98WR02406>
- Pizarro, G., & Lall, U. (2002). El Niño-induced flooding in the U.S. West: What can we expect? *Eos, Transactions, American Geophysical Union*, 83(32), 349. <https://doi.org/10.1029/2002EO000255>
- Prairie, J., Rajagopalan, B., Lall, U., & Fulp, T. (2007). A stochastic nonparametric technique for space-time disaggregation of streamflows. *Water Resources Research*, 43, W03432. <https://doi.org/10.1029/2005WR004721>
- Probst, J. L., & Tardy, Y. (1987). Long range streamflow and world continental runoff fluctuations since the beginning of this century. *Journal of Hydrology*, 94(3–4), 289–311. [https://doi.org/10.1016/0022-1694\(87\)90057-6](https://doi.org/10.1016/0022-1694(87)90057-6)
- Radziejewski, M., & Kundzewicz, Z. W. (2004). Detectability of changes in hydrological records/Possibilité de détecter les changements dans les chroniques hydrologiques. *Hydrological Sciences Journal*, 49(1), 39–51. <https://doi.org/10.1623/hysj.49.1.39.54002>
- Ritchie, J. W., Zammitt, C., & Beal, D. (2004). Can seasonal climate forecasting assist in catchment water management decision-making? *Agriculture, Ecosystems & Environment*, 104(3), 553–565. <https://doi.org/10.1016/j.agee.2004.01.029>
- Ropelewski, C. F., & Halpert, M. S. (1986). North American precipitation and temperature patterns associated with the El Niño/Southern Oscillation (ENSO). *Monthly Weather Review*, 114(12), 2352–2362. [https://doi.org/10.1175/1520-0493\(1986\)114<2352:NAPATP>2.0.CO;2](https://doi.org/10.1175/1520-0493(1986)114<2352:NAPATP>2.0.CO;2)
- Ropelewski, C. F., & Halpert, M. S. (1987). Global and regional scale precipitation patterns associated with the El Niño/Southern Oscillation. *Monthly Weather Review*, 115(8), 1606–1626. [https://doi.org/10.1175/1520-0493\(1987\)115<1606:GARSPPP>2.0.CO;2](https://doi.org/10.1175/1520-0493(1987)115<1606:GARSPPP>2.0.CO;2)
- Sankarasubramanian, A., & Lall, U. (2003). Flood quantiles in a changing climate: Seasonal forecasts and causal relations. *Water Resources Research*, 39, 1134. <https://doi.org/10.1029/2002WR001593>
- Shanahan, T. M., Overpeck, J. T., Anchukaitis, K. J., Beck, J. W., Cole, J. E., Dettman, D. L., et al. (2009). Atlantic forcing of persistent drought in West Africa. *Science*, 324(5925), 377–380. <https://doi.org/10.1126/science.1166352>
- Shukla, S., & Lettenmaier, D. P. (2011). Seasonal hydrologic prediction in the United States: Understanding the role of initial hydrologic conditions and seasonal climate forecast skill. *Hydrology and Earth System Sciences*, 15(11), 3529–3538. <https://doi.org/10.5194/hess-15-3529-2011>
- Sittichok, K., Djibo, A. G., Seidou, O., Saley, H. M., Karambiri, H., & Paturel, J. (2016). Statistical seasonal rainfall and streamflow forecasting for the Sirba watershed, West Africa, using sea-surface temperatures. *Hydrological Sciences Journal*, 61, 805–815. <https://doi.org/10.1080/02626667.2014.944526>
- Sun, C., Li, J., Feng, J., & Xie, F. (2015). A decadal-scale teleconnection between the North Atlantic Oscillation and Subtropical Eastern Australian Rainfall. *Journal of Climate*, 28(3), 1074–1092. <https://doi.org/10.1175/JCLI-D-14-00372.1>
- Tootle, G. A., & Piechota, T. C. (2004). Suwannee river long range streamflow forecasts based on seasonal climate predictors. *Journal of the American Water Resources Association*, 40(2), 523–532. <https://doi.org/10.1111/j.1752-1688.2004.tb01047.x>
- Tootle, G. A., Piechota, T. C., & Singh, A. (2005). Coupled oceanic-atmospheric variability and U.S. streamflow. *Water Resources Research*, 41, W12408. <https://doi.org/10.1029/2005WR004381>
- Uppala, S. M., Källberg, P. W., Simmons, A. J., Andrae, U., Da Costa Bechtold, V., Fiorino, M., et al. (2005). The ERA-40 re-analysis. *Quarterly Journal of the Royal Meteorological Society*, 131(612), 2961–3012. <https://doi.org/10.1256/qj.04.176>
- Van Beek, L. P. H., & Bierkens, M. F. P. (2009). *The global hydrological model PCR-GLOBWB: Conceptualization, parameterization and verification*. The Netherlands: Utrecht University.
- Van Beek, L. P. H., Wada, Y., & Bierkens, M. F. P. (2011). Global monthly water stress: 1. Water balance and water availability. *Water Resources Research*, 47, W07517. <https://doi.org/10.1029/2010WR009791>
- van Dijk, A. I. J. M., Peña-Arancibia, J. L., Wood, E. F., Sheffield, J., & Beck, H. E. (2013). Global analysis of seasonal streamflow predictability using an ensemble prediction system and observations from 6192 small catchments worldwide. *Water Resources Research*, 49, 2729–2746. <https://doi.org/10.1002/wrcr.20251>
- Wada, Y., van Beek, L. P. H., Viviroli, D., Dürr, H. H., Weingartner, R., & Bierkens, M. F. P. (2011). Global monthly water stress: 2. Water demand and severity of water stress. *Water Resources Research*, 47, W07518. <https://doi.org/10.1029/2010WR009792>
- Wanders, N., & Wada, Y. (2015). Decadal predictability of river discharge with climate oscillations over the 20th and early 21st century. *Geophysical Research Letters*, 42, 10689–10695. <https://doi.org/10.1002/2015GL066929>
- Ward, P. J., Beets, W., Bouwer, L. M., Aerts, J. C. J. H., & Renssen, H. (2010). Sensitivity of river discharge to ENSO. *Geophysical Research Letters*, 37, L12402. <https://doi.org/10.1029/2010GL043215>

- Ward, P. J., Eisner, S., Flörke, M., Dettinger, M. D., & Kummu, M. (2014a). Annual flood sensitivities to El Niño-Southern Oscillation at the global scale. *Hydrology and Earth System Sciences*, 18(1), 47–66. <https://doi.org/10.5194/hess-18-47-2014>
- Ward, P. J., Jongman, B., Kummu, M., Dettinger, M. D., Sperna Weiland, F. C., & Winsemius, H. C. (2014b). Strong influence of El Niño Southern Oscillation on flood risk around the world. *Proceedings of the National Academy of Sciences of the United States of America*, 111(44), 15659–15664. <https://doi.org/10.1073/pnas.1409822111>
- Ward, P. J., Jongman, B., Weiland, F. S., Bouwman, A., van Beek, R., Bierkens, M. F. P., et al. (2013). Assessing flood risk at the global scale: Model setup, results, and sensitivity. *Environmental Research Letters*, 8(4), 44019. <https://doi.org/10.1088/1748-9326/8/4/044019>
- World Commission on Dams (WCD) (2000). *Dams and development: A framework for decision making*. London, UK: Earthscan.
- Weedon, G. P., Gomes, S., Viterbo, P., Shuttleworth, W. J., Blyth, E., Österle, H., et al. (2011). Creation of the WATCH forcing data and its use to assess global and regional reference crop evaporation over land during the twentieth century. *Journal of Hydrometeorology*, 12(5), 823–848. <https://doi.org/10.1175/2011JHM1369.1>
- Werner, K., Brandon, D., Clark, M., & Gangopadhyay, S. (2004). Climate index weighting schemes for NWS ESP-based seasonal volume forecasts. *Journal of Hydrometeorology*, 5(6), 1076–1090. <https://doi.org/10.1175/JHM-381.1>
- Westra, S., & Sharma, A. (2010). An upper limit to seasonal rainfall predictability? *Journal of Climate*, 23(12), 3332–3351. <https://doi.org/10.1175/2010JCLI3212.1>
- Wilks, D. S. (2011). *Statistical methods in the atmospheric sciences*. Cambridge, MA: Academic Press.
- Winsemius, H. C., Van Beek, L. P. H., Jongman, B., Ward, P. J., & Bouwman, A. (2013). A framework for global river flood risk assessments. *Hydrology and Earth System Sciences*, 17(5), 1871–1892. <https://doi.org/10.5194/hess-17-1871-2013>
- World Meteorological Organization (2007). Manual on the global data processing and forecasting systems. In *Standard Verification System (SVS) for Long-Range Forecasts (LRF)*. Geneva, Switzerland: World Meteorological Organization
- Zhang, R., & Delworth, T. L. (2006). Impact of Atlantic multidecadal oscillations on India/Sahel rainfall and Atlantic hurricanes. *Geophysical Research Letters*, 33, L17712. <https://doi.org/10.1029/2006GL026267>
- Zhang, Y., Moges, S., & Block, P. (2018). Does objective cluster analysis serve as a useful precursor to seasonal precipitation prediction at local scale? Application to western Ethiopia. *Hydrology and Earth System Sciences*, 22(1), 143–157. <https://doi.org/10.5194/hess-22-143-2018>
- Zhang, Y., Wallace, J. M., & Battisti, D. S. (1997). ENSO-like interdecadal variability: 1900–93. *Journal of Climate*, 10, 1004–1020. [https://doi.org/10.1175/1520-0442\(1997\)010<1004:ELIV>2.0.CO;2](https://doi.org/10.1175/1520-0442(1997)010<1004:ELIV>2.0.CO;2)